applied sciences

MDPI

Article

Improved Temporal Fuzzy Reasoning Spiking Neural P Systems for Power System Fault Diagnosis

Ning Shao, Qing Chen *, Dan Xie, Ye Sun and Chengao Yu

Key Laboratory of Power System Intelligent Dispatch and Control of Ministry of Education, Shandong University, Jinan 250061, China; 202020548@mail.sdu.edu.cn (N.S.); 202114600@mail.sdu.edu.cn (D.X.); 202134689@mail.sdu.edu.cn (Y.S.); 202134719@mail.sdu.edu.cn (C.Y.)

* Correspondence: qchen@sdu.edu.cn

Abstract: Fuzzy and temporal reasoning can effectively improve the accuracy of fault diagnosis methods. However, there are challenges in practical applications, such as missing alarm messages, temporal reasoning with complex calculations, and complex modeling processes. Therefore, this study proposes an improved temporal fuzzy reasoning spiking neural P (ITFRSNP) system for power system fault diagnosis. First, the ITFRSNP system and its reasoning method are proposed to perform association reasoning between confidence degrees and temporal constraints. Second, a general fault diagnosis model and process are developed based on the ITFRSNP system to diagnose various faulty components and simplify the modeling process. In addition, a search method is provided for identifying suspected faulty components, considering the missing alarm message of the circuit breaker. Simulation results of fault cases demonstrate that the proposed method exhibits high accuracy and fault tolerance. It can precisely identify faulty components despite incorrect operations or inaccurate alarm messages of protective relays and circuit breakers. Moreover, the search method effectively narrows down the diagnostic scope without missing suspected faulty components in scenarios where alarms from boundary circuit breakers are missing, thereby enhancing the fault diagnosis efficiency. The fault diagnosis model features a straightforward structure and reasoning process with minimal computational complexity, making it suitable for real-time diagnosis of complex faults within power systems.

Keywords: power system; fault diagnosis; temporal reasoning; improved temporal fuzzy reasoning spiking neural P system; general fault diagnosis model

check for updates

Citation: Shao, N.; Chen, Q.; Xie, D.; Sun, Y.; Yu, C. Improved Temporal Fuzzy Reasoning Spiking Neural P Systems for Power System Fault Diagnosis. *Appl. Sci.* **2024**, *14*, 1753. https://doi.org/10.3390/app14051753

Received: 21 January 2024
Revised: 11 February 2024
Accepted: 19 February 2024
Published: 21 February 2024

Copyright: © 2024 by the authors. Licensee MDPI, Basel, Switzerland. This article is an open access article distributed under the terms and conditions of the Creative Commons Attribution (CC BY) license (https://creativecommons.org/licenses/by/4.0/).

1. Introduction

Faults are inevitable during the operation of a power system. Therefore, power systems are equipped with many protective relays (PRs) and circuit breakers (CBs), which quickly, reliably, and selectively isolate faults, limit the extent of power outages, and reduce economic loss. After a fault occurs, alarm messages from the PRs and CBs are reported to the dispatch center, providing important decision-making support for regulating and operating power systems. Rapid and accurate diagnosis of faulty components is essential for the rapid restoration of power supply, reducing the influence scope of the accident, and ensuring the safety and stability of the power system. Achieving this goal not only effectively reduces the duration of power outages and ensures normal social production and residential life but also reduces the economic losses caused by power outages. In addition, efficient fault diagnosis methods provide important decision support for the maintenance and improvement of the power system, thereby improving the efficiency and accuracy of fault resolution and establishing a solid foundation for the long-term stable operation of the power system.

Recently, experts and scholars have proposed various fault diagnosis methods based on alarm messages, including expert systems [1,2], analytical models [3–5], artificial neu-

ral networks [6,7], Bayesian networks [8,9], Petri nets [10–13], and spiking neural P systems [14,15]. Expert systems match alarm messages with a knowledge base to identify faulty components. The knowledge base of an expert system is difficult to build and maintain for a large-scale power system, and its generalizability and fault tolerance must be improved. The analytical model constructs a mathematical model that expresses the logical relationship between components, PRs, and CBs, according to the protection configuration and operation rules. It represents the fault diagnosis problem as an integer programming problem, and then applies an intelligent optimization algorithm to find the fault hypothesis that best explains the alarm messages. Artificial neural networks represent the causal relationships between alarm information and faulty components using high-order nonlinear equations. However, artificial neural networks require many training samples, and their portability is poor. Bayesian networks involve considerable effort to determine prior probabilities and face difficulties in online applications without automated modeling techniques. Petri nets graphically explain the topology of the grid and use mathematical methods to reason and analyze the logical relationships between components, PRs, and CBs implied in fault messages. Petri nets require reconstruction or adjustment of their fault diagnosis models to accommodate topological changes, complicating the modeling process.

The concept of a fault diagnosis method utilizing a spiking neural P (SNP) system was first proposed in 2013. The SNP system employs synapses to connect propositions and rule neurons, thereby delineating the relationships between faulty components, PRs, and CBs. The confidence degrees of PRs and CBs follow the spikes passing along the synapses between neurons to simulate the dynamic process of fault isolation. Notably, SNP systems do not require training and can explicitly describe the causal logic among components, PRs, and CBs, demonstrating commendable fault tolerance, flexibility, and scalability. Nonetheless, the potential for PRs and CBs to malfunction or cease functioning, coupled with the possibility of false alarms and omissions in their alarm messages, complicates fault diagnosis due to the uncertainty of operational states and alarm messages. In response, enhanced models and schemes for SNP systems have been proposed to address problems faced in practical fault diagnosis applications. Owing to the uncertainty of alarm messages, scholars have adopted trapezoidal fuzzy numbers [16], intuitionistic fuzzy numbers [17], and interval-valued fuzzy numbers [18] to characterize the operational states of PRs and CBs, thereby improving the accuracy of the diagnosis results. Moreover, a combination of biological apoptosis mechanisms and rough sets has been applied [19] to simplify the fault diagnosis model and manage the uncertainty and incompleteness of alarm messages.

The study referenced in [20] employs the temporal constraints between fault occurrence and operation times of PRs or CBs to distinguish between valid and invalid alarm messages. It assigns confidence degrees to valid alarm messages based on their temporal constraints and correspondence. Subsequently, ref. [21] introduced causal networks to identify PRs and CBs that do not conform to these temporal constraints, enabling adjustments to their confidence degrees. The research in [22] developed the time sequence spiking neural P system with real numbers (rTSSNPS), which facilitates the logical association of confidence levels with temporal constraints. The temporal features of the alarm message are introduced in [20–22] to prevent non-faulty components from being misclassified as faulty components and enhance the accuracy of the fault diagnosis results. However, the above methods encounter limitations in practical applications: (1) The modeling process is complicated by traversing all the suspected faulty components to construct fault diagnosis models, and these models need to be reconstructed when adapting to topology changes. (2) The missing alarm message of the CB reduces the accuracy and fault tolerance of fault diagnosis results. Moreover, the outage area may not be recognized, and all components in the power grid need to be diagnosed, which seriously affects the efficiency of fault diagnosis.

To solve these problems, this study proposes a fault diagnosis method based on an improved temporal fuzzy reasoning spiking neural P (ITFRSNP) system. The main contributions of this study are as follows:

1. The ITFRSNP system and its associated reasoning algorithm are proposed. The ITFRSNP system contains new rule neurons and reasoning methods, simplifying the correlation reasoning of confidence degrees and temporal features. The ITFRSNP system can effectively improve the accuracy and fault tolerance of fault diagnosis. This lays a theoretical foundation for constructing a general fault diagnosis model and its diagnosis reasoning method.
2. The CB subnet is defined based on the configuration of the CBs and corresponding protections. A general fault diagnosis model and its fault diagnosis process are developed based on the ITFRSNP system for CB subnets. The proposed model simplifies the modeling process and can be directly applied to fault diagnosis of various components with good versatility and adaptability.
3. A search method for suspected faulty components is proposed. The search method does not need to traverse the entire power system and does not miss suspected faulty components. This method narrows the scope of topology search and fault diagnosis and can effectively improve the efficiency of fault diagnosis.

The remainder of this study is organized as follows. Section 2 defines the ITFRSNP system and its reasoning algorithms. Section 3 describes the fault diagnosis method based on the ITFRSNP system. Section 4 presents the fault case validation and algorithm comparison, and Section 5 concludes this study.

2. ITFRSNP System

This section proposes the ITFRSNP system with new rule neurons and a reasoning algorithm. This section provides a theoretical foundation for a general fault diagnosis model and its diagnosis process.

2.1. Temporal Constraints and Temporal Reasonings

The temporal constraints are defined as follows [10]:

1. The time-point constraint (T(a) = [t_a^-, t_a^+]) indicates that event a occurs in the time interval [t_a^-, t_a^+]. If $t_a^- = t_a^+$, event a occurs at a specific time.
2. The time-distance constraint (D(a, b) = [Δt_{ab}^-, Δt_{ab}^+]) indicates that the time distance between the occurrence times of events a and b is within the time interval [Δt_{ab}^-, Δt_{ab}^+].

According to the above definitions, the following are temporal reasonings that utilize the interval calculation rules.

1. Reverse reasoning: The time-point constraint T(b) and the time-distance constraint D(a, b) are known. The following definition can be employed to infer the time-point constraint T(a):

$$T(\mathrm{a}) = T(\mathrm{b}) - D(\mathrm{a},\mathrm{b}) = [t_{\mathrm{b}}^- - \Delta t_{\mathrm{ab}}^+, t_{\mathrm{b}}^+ - \Delta t_{\mathrm{ab}}^-] \quad (1)$$

2. Merge reasoning: If event a is known to satisfy multiple time-point constraints T_1(a), T_2(a), T_3(a), …, T_k(a) simultaneously, the following definition can be employed to infer the time-point constraint T(a).

$$T(\mathrm{a}) = T_1(\mathrm{a}) \cap T_2(\mathrm{a}) \cap \cdots \cap T_k(\mathrm{a}) \quad (2)$$

2.2. The TFRSNP System

The ITFRSNP system is defined as follows:

$$\Pi = (A, N_p, N_r, syn, I, O) \quad (3)$$

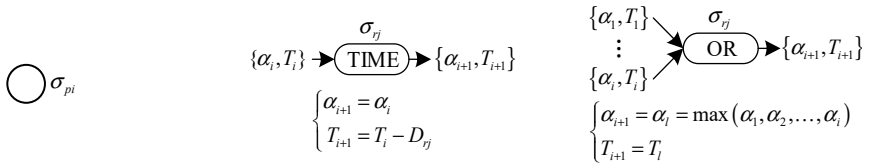
where the following are defined:

1. $A = \{a\}$ is a singleton alphabet (a is called spike).
2. $N_p = \{\sigma_{p1}, \sigma_{p2}, \ldots, \sigma_{pm}\}$ denotes the proposition neuron set, where σ_{pi} $(1 \leq i \leq m)$ is associated with a fuzzy proposition. Each proposition neuron σ_{pi} has the form $\sigma_{pi} = (\alpha_{pi}, T_{pi}, \theta_{pi}, \lambda_{pi}, r_{pi})$, where the following are defined:
   a. α_{pi} ($\alpha_{pi} \in [0, 1]$) is the spike value in σ_{pi};
   b. T_{pi} ($T_{pi} = [{t_{pi}}^{-}, {t_{pi}}^{+}]$) is the time-point constraint in σ_{pi};
   c. θ_{pi} is an integer representing the number of spikes received by σ_{pi};
   d. λ_{pi} is an integer that represents the spike number threshold required for firing σ_{pi};
   e. r_{pi} is a firing/spiking rule of σ_{pi} with the form $E/a^{\theta} \rightarrow a^{\beta}$, where θ and β are real numbers in [0, 1].
3. $N_r = \{\sigma_{r1}, \sigma_{r2}, \ldots, \sigma_{rn}\}$ is the rule neuron set, where σ_{rj} $(1 \leq j \leq n)$ is associated with a fuzzy production rule. N_r contains two types of rule neurons: TIME-type and OR-type. Each rule neuron σ_{rj} has the form $\sigma_{rj} = (\alpha_{rj}, T_{rj}, D_{rj}, \theta_{rj}, \lambda_{rj}, r_{rj})$, where:
   a. α_{rj} ($\alpha_{rj} \in [0, 1]$) is the spike value in σ_{rj};
   b. T_{rj} ($T_{rj} = [{t_{rj}}^{-}, {t_{rj}}^{+}]$) is the time-point constraint in σ_{rj};
   c. D_{rj} ($D_{rj} = [\Delta{t_{rj}}^{-}, \Delta{t_{rj}}^{+}]$) is the time-distance constraint in σ_{rj}, which denotes the time-distance constraint between the propositions of the input and output proposition neurons associated with σ_{rj};
   d. θ_{rj} is an integer representing the number of spikes received by σ_{rj};
   e. λ_{rj} is an integer that represents the spike number threshold required for firing σ_{rj};
   f. r_{rj} is a firing/spiking rule of σ_{rj}, with the form $E/\mathrm{a}^{\theta} \rightarrow \mathrm{a}^{\beta}$, where θ and β are real numbers in [0, 1].
4. $syn \subseteq \{N_p \times N_r\} \cup \{N_p \times N_r\}$ is a directed graph that indicates the synapses between propositions and rule neurons. Input matrices $\boldsymbol{U}_1 = \{u_{1(i,j)}\}_{m \times n}$ and $\boldsymbol{U}_2 = \{u_{2(i,j)}\}_{m \times n}$ and output matrix $\boldsymbol{V} = \{v_{(j,i)}\}_{n \times m}$, where $u_{1(i,j)}$, $u_{2(i,j)}$, and $v_{(i,j)} \in [0, 1]$, are used to represent syn. If there is a synapse from proposition neuron σ_{pi} to TIME-type neuron σ_{rj}, then $u_{1(i,j)} = 1$; otherwise, $u_{1(i,j)} = 0$. If there is a synapse from proposition neuron σ_{pi} to OR-type neuron σ_{rj}, then $u_{2(i,j)} = 1$; otherwise, $u_{2(i,j)} = 0$. If there is a directed arc (synapse) from rule neuron σ_{rj} to proposition neuron σ_{pi}, then $v_{(j,i)} = 1$; otherwise, $v_{(j,i)} = 0$.
5. I and O are input and output neuron sets, respectively.

Graphical models of the proposition neuron, TIME-type rule neuron, and OR-type rule neuron are shown in Figure 1. Their respective interpretations are provided below:

1. The proposition neuron (Figure 1a) describes the operational events of PRs and CBs. When a PR alarm message is received, the spike value in the proposition neuron corresponds to its confidence degree, and the time-point constraint corresponds to its operation time. The proposition neuron can delineate the state and time of the PR and CB operations, which are then inputted into the fault diagnosis model for inference. Moreover, this neuron can record the intermediate and output results of the fault diagnosis.
2. The TIME-type rule neuron (Figure 1b) receives spikes from the proposition neuron. It then transmits the spike value to the next proposition neuron, and deduces the time-point constraints backward according to Equation (1) before forwarding them. This rule neuron is responsible for characterizing the temporal distance constraints between propositions that correspond to their associated propositional neurons. The TIME-type rule neurons employ reverse reasoning to deduce the time-point constraints for the PRs from those of the corresponding CBs and their time-distance constraints. Similarly, they apply to determine the time-point constraints of the faults by leveraging the time-point constraints and time-distance constraints of the PRs.

3. The OR-type rule neuron (Figure 1c) receives spikes from the proposition neurons and takes the maximum spike value α_l and the corresponding time-point constraint T_l to transmit to the next proposition neuron. Each component is equipped with multiple sets of protections, including primary, near backup, and remote backup protections. The OR-type rule neuron determines the protection type for isolating the faulty component by selecting the PR and CB with the highest confidence degree.



(**a**) (**b**) (**c**)

Figure 1. Three types of neurons: (**a**) proposition neuron, (**b**) TIME-type rule neuron, and (**c**) OR-type rule neuron.

2.3. The Reasoning Algorithm of the ITFRSNP System

Before describing the reasoning algorithm for the ITFRSNP system, the definitions of the matrices and vectors used in the reasoning process are first introduced.

1. $\boldsymbol{\alpha_p} = (\alpha_{p1}, \alpha_{p2}, \ldots, \alpha_{pm})^{\mathrm{T}}$ and $\boldsymbol{\alpha_r} = (\alpha_{r1}, \alpha_{r2}, \ldots, \alpha_{rn})^{\mathrm{T}}$ are vectors consisting of spike values in m proposition and n rule neurons, respectively. α_{pi} $(1 \leq i \leq m)$ and α_{rj} $(1 \leq j \leq n)$ represent the spike values of the i-th proposition neuron and j-th rule neuron, respectively. This relationship between the vector elements and neurons applies to the subsequent vector definitions as well.
2. $\boldsymbol{T_p} = (T_{p1}, T_{p2}, \ldots, T_{pm})^{\mathrm{T}}$ and $\boldsymbol{T_r} = (T_{r1}, T_{r2}, \ldots, T_{rn})^{\mathrm{T}}$ are vectors consisting of time-point constraints in m proposition and n rule neurons, respectively.
3. $\boldsymbol{D_r} = (D_{r1}, D_{r2}, \ldots, D_{rn})^{\mathrm{T}}$ is a vector of the time-distance constraints in n rule neurons.
4. $\boldsymbol{\theta_p} = (\theta_{p1}, \theta_{p2}, \ldots, \theta_{pm})^{\mathrm{T}}$ and $\boldsymbol{\theta_r} = (\theta_{r1}, \theta_{r2}, \ldots, \theta_{rn})^{\mathrm{T}}$ are vectors consisting of spike numbers in m proposition and n rule neurons, respectively.
5. $\boldsymbol{\lambda_p} = (\lambda_{p1}, \lambda_{p2}, \ldots, \lambda_{pm})^{\mathrm{T}}$ and $\boldsymbol{\lambda_r} = (\lambda_{r1}, \lambda_{r2}, \ldots, \lambda_{rn})^{\mathrm{T}}$ are vectors consisting of spike number thresholds in m proposition and n rule neurons, respectively.
6. $\boldsymbol{\beta}_p = (\beta_{p1}, \beta_{p2}, \ldots, \beta_{pm})^{\mathrm{T}}$ and $\boldsymbol{\beta}_r = (\beta_{r1}, \beta_{r2}, \ldots, \beta_{rn})^{\mathrm{T}}$ are vectors consisting of spike values output from m proposition neurons and n rule neurons, respectively.
7. $\boldsymbol{\tau}_p = (\tau_{p1}, \tau_{p2}, \ldots, \tau_{pm})^{\mathrm{T}}$ and $\boldsymbol{\tau}_r = (\tau_{r1}, \tau_{r2}, \ldots, \tau_{rn})^{\mathrm{T}}$ are vectors consisting of time-point constraints output from m proposition and n rule neurons, respectively, after firing.
8. $\boldsymbol{b}_p = (b_{p1}, b_{p2}, \ldots, b_{pm})^{\mathrm{T}}$ and $\boldsymbol{b}_r = (b_{r1}, b_{r2}, \ldots, b_{rn})^{\mathrm{T}}$ are vectors consisting of spike numbers output from m proposition neurons and n rule neurons, respectively, after firing.
9. $\boldsymbol{B_p} = \mathrm{diag}(b_p)$ and $\boldsymbol{B_r} = \mathrm{diag}(b_r)$ are diagonal matrices, where diag( ) is the diagonal function.

The following matrix calculation rules are defined by incorporating temporal reasoning into fuzzy reasoning.

1. $\boldsymbol{H} = \boldsymbol{C} * \boldsymbol{D}$:

$$H_i = \bigcap_{\mathbf{C}_{ik} \neq 0, 1 \leq k \leq t} D_k \tag{4}$$

where $\boldsymbol{D}$ and $\boldsymbol{H}$ are $t \times 1$-and $s \times 1$-dimensional vectors of time-distance constraints, respectively, and $\boldsymbol{C}$ is an $s \times t$-dimensional binary matrix.

2. $\boldsymbol{J} = \boldsymbol{G} - \boldsymbol{H}$:

$$J_i = G_i - H_i \tag{5}$$

where $\boldsymbol{G}$ and $\boldsymbol{J}$ are $s \times 1$-dimensional vectors of time-point constraints.

3. $\{\boldsymbol{P}, \boldsymbol{Q}\} = \{\boldsymbol{C}, \boldsymbol{D}\} \oplus \{\boldsymbol{F}, \boldsymbol{G}\}$:

$$\begin{cases} \boldsymbol{P} = \boldsymbol{C}^{\mathrm{T}} \times \boldsymbol{F} \\ Q_i = \underset{C_{ik}^{\mathrm{T}} \neq 0, 1 \leq k \leq s}{\cap} (\boldsymbol{G} - \boldsymbol{C} * \boldsymbol{D})_k \end{cases} \tag{6}$$

where $\boldsymbol{F}$ and $\boldsymbol{P}$ are $s \times 1$ and $t \times 1$-dimensional vectors of spike values, and $\boldsymbol{Q}$ is a $t \times 1$-dimensional vector of time-point constraints.

4. $\{\boldsymbol{P}, \boldsymbol{Q}\} = \{\mathbf{C}, \boldsymbol{D}\} \otimes \{\boldsymbol{F}, \boldsymbol{G}\}$:

$$\begin{cases} P_i = \underset{C_{ik}^{\mathrm{T}} \neq 0, 1 \leq k \leq s}{\max} (F_k) \\ Q_i = G_j, \quad 1 \leq j \leq s, F_j = P_i \end{cases} \tag{7}$$

5. $\{\boldsymbol{P}, \boldsymbol{Q}\} = \{\mathbf{P}', \mathbf{Q}'\} \widehat{\times} \{\boldsymbol{P}'', \boldsymbol{Q}''\}$:

$$\begin{cases} P_i = \max(P'_i, P''_i) \\ Q_i = Q'_i \cup Q''_i \end{cases} \tag{8}$$

where $\boldsymbol{P}'$ and $\boldsymbol{P}''$ are $t \times 1$-dimensional vectors of the spike values, and Q' and Q'' are $t \times 1$-dimensional vectors of the time-point constraints.

6. $\{\boldsymbol{P}, \boldsymbol{Q}\} = \{\boldsymbol{P}', \boldsymbol{Q}'\} \widehat{+} \{\boldsymbol{P}'', \boldsymbol{Q}''\}$:

$$P_i = \begin{cases} \mathrm{avg}(P'_i, P''_i), & P'_i \neq 0 \\ P''_i, & P'_i = 0 \end{cases} \tag{9}$$

$$Q_i = \begin{cases} Q'_i \cap Q''_i, & Q'_i \cap Q''_i \neq \varnothing \\ Q'_i \cup Q''_i, & Q'_i \cap Q''_i = \varnothing \end{cases} \tag{10}$$

7. $\{\boldsymbol{\beta}, \boldsymbol{\tau}\} = \mathrm{fire}\ (\boldsymbol{\alpha}, \boldsymbol{T}, \boldsymbol{\theta}, \boldsymbol{\lambda})$:

$$\beta_i = \begin{cases} \alpha_i, & \theta_i = \lambda_i \\ 0, & \theta_i < \lambda_i \end{cases} \tag{11}$$

$$\tau_i = \begin{cases} T_i, & \theta_i = \lambda_i \\ \varnothing, & \theta_i < \lambda_i \end{cases} \tag{12}$$

8. $\{\boldsymbol{\alpha}, \boldsymbol{T}\} = \mathrm{update}\ (\boldsymbol{\alpha}, \boldsymbol{T}, \boldsymbol{\theta}, \boldsymbol{\lambda})$:

$$\alpha_i = \begin{cases} \alpha_i, & 0 < \theta_i < \lambda_i \\ 0, & \theta_i = 0 \text{ or } \theta_i = \lambda_i \end{cases} \tag{13}$$

$$T_i = \begin{cases} T_i, & 0 < \theta_i < \lambda_i \\ \varnothing, & \theta_i = 0 \text{ or } \theta_i = \lambda_i \end{cases} \tag{14}$$

9. $\boldsymbol{b} = \mathrm{fire}\ (1, \boldsymbol{\theta}, \boldsymbol{\lambda})$:

$$\beta_i = \begin{cases} 1, & \theta_i = \lambda_i \\ 0, & \theta_i < \lambda_i \end{cases} \tag{15}$$

10. $\boldsymbol{\theta} = \mathrm{update}\ (\boldsymbol{\theta}, \boldsymbol{\theta}, \boldsymbol{\lambda})$:

$$\theta_i = \begin{cases} 0, & \theta_i = \lambda_i \\ \theta_i, & \theta_i < \lambda_i \end{cases} \tag{16}$$

Based on the matrix calculation rules, the reasoning algorithm for the ITFRSNP system is as follows.

1. Input parameter matrices and vectors $\boldsymbol{U}_1$, $\boldsymbol{U}_2$, $\boldsymbol{V}$, $\boldsymbol{\lambda_p}$, $\boldsymbol{\lambda_r}$, $\boldsymbol{D_r}$, $\boldsymbol{\theta_p}$, and $\boldsymbol{\theta_r}$. The number of interactive inferences is g, and the vectors of the spike values and time-point constraints in the g-th iteration are $\boldsymbol{\alpha}_p^g$, $\mathbf{T}_p^g$, $\boldsymbol{\alpha}_r^g$, and $\mathbf{T}_r^g$. Initialize the number of iterations $g = 0$ and input $\boldsymbol{\alpha}_p^0$, $\mathbf{T}_p^0$, $\boldsymbol{\alpha}_r^0$, and $\mathbf{T}_r^0$.

2. Process the firing of proposition neurons:

$$\begin{cases} \left\{\boldsymbol{\beta}_p^g, \boldsymbol{\tau}_p^g\right\} = \text{fire}(\boldsymbol{\alpha}_p^g, \boldsymbol{T}_p^g, \boldsymbol{\theta}_p^g, \boldsymbol{\lambda}_p) \\ \boldsymbol{b}_p^g = \text{fire}(1, \boldsymbol{\theta}_p^g, \boldsymbol{\lambda}_p) \\ \boldsymbol{B}_p^g = \text{diag}(\boldsymbol{b}_p^g) \\ \left\{\boldsymbol{\alpha}_p^g, \boldsymbol{T}_p^g\right\} = \text{update}(\boldsymbol{\alpha}_p^g, \boldsymbol{T}_p^g, \boldsymbol{\theta}_p^g, \boldsymbol{\lambda}_p) \\ \boldsymbol{\theta}_p^g = \text{update}(\boldsymbol{\theta}_p^g, \boldsymbol{\theta}_p^g, \boldsymbol{\lambda}_p) \end{cases} \tag{17}$$

3. Compute $\boldsymbol{\alpha}_r^{g+1}$, $\boldsymbol{T}_r^{g+1}$ and $\boldsymbol{\theta}_r^{g+1}$:

$$\begin{cases} \left\{\boldsymbol{\alpha}_r^{g+1}, \boldsymbol{T}_r^{g+1}\right\} = \left(\left\{(\boldsymbol{B}_p^g \cdot \boldsymbol{U}_1), \boldsymbol{D}_r\right\} \oplus \left\{\boldsymbol{\beta}_p^g, \boldsymbol{\tau}_p^g\right\}\right) \widehat{\times} \left(\left\{(\boldsymbol{B}_p^g \cdot \boldsymbol{U}_2), \boldsymbol{D}_r\right\} \otimes \left\{\boldsymbol{\beta}_p^g, \boldsymbol{\tau}_p^g\right\}\right) \\ \boldsymbol{\theta}_r^{g+1} = \boldsymbol{\theta}_r^g + \left\{\left[\boldsymbol{B}_p^g \cdot (\boldsymbol{U}_1 + \mathbf{U}_2)\right]^{\mathrm{T}} \times \boldsymbol{b}_p^g\right\} \end{cases} \tag{18}$$

4. Process the firing of rule neurons:

$$\begin{cases} \left\{\boldsymbol{\beta}_r^{g+1}, \boldsymbol{\tau}_r^{g+1}\right\} = \text{fire}(\boldsymbol{\alpha}_r^{g+1}, \boldsymbol{T}_r^{g+1}, \boldsymbol{\theta}_r^{g+1}, \boldsymbol{\lambda}_r) \\ \boldsymbol{b}_r^{g+1} = \text{fire}(1, \boldsymbol{\theta}_r^{g+1}, \boldsymbol{\lambda}_r) \\ \boldsymbol{B}_r^{g+1} = \text{diag}(\boldsymbol{b}_r^{g+1}) \\ \left\{\boldsymbol{\alpha}_r^{g+1}, \boldsymbol{T}_r^{g+1}\right\} = \text{update}(\boldsymbol{\alpha}_r^{g+1}, \boldsymbol{T}_r^{g+1}, \boldsymbol{\theta}_r^{g+1}, \boldsymbol{\lambda}_r) \\ \boldsymbol{\theta}_r^{g+1} = \text{update}(\boldsymbol{\theta}_r^{g+1}, \boldsymbol{\theta}_r^{g+1}, \boldsymbol{\lambda}_r) \end{cases} \tag{19}$$

5. Compute $\boldsymbol{\alpha}_p^{g+1}$, $\boldsymbol{T}_p^{g+1}$ and $\boldsymbol{\theta}_p^{g+1}$:

$$\begin{cases} \{\boldsymbol{\alpha}_p^{g+1}, \boldsymbol{T}_p^{g+1}\} = \{\boldsymbol{\alpha}_p^g, \boldsymbol{T}_p^g\} \widehat{+} [\{(\boldsymbol{V} \cdot \boldsymbol{B}_r^{g+1}), \boldsymbol{D}_r\} \otimes \{\boldsymbol{\beta}_r^g, \boldsymbol{\tau}_r^g\}] \\ \boldsymbol{\theta}_p^{g+1} = \boldsymbol{\theta}_p^g + [(\boldsymbol{V} \cdot \boldsymbol{B}_r^{g+1})^{\mathrm{T}} \times \boldsymbol{b}_r^g] \end{cases} \tag{20}$$

6. If $\boldsymbol{\theta}_p^{g+1} = (0, 0, \ldots, 0)^{\mathrm{T}}$ and $\boldsymbol{\theta}_r^{g+1} = (0, 0, \ldots, 0)^{\mathrm{T}}$, then halt and export reasoning results ($\boldsymbol{\alpha}_p^g$ and $\boldsymbol{T}_p^g$); otherwise, $g = g + 1$ and return to Step 2.

2.4. Comparison between ITFRSNP and RTSSNPS Systems

In Sections 2.2 and 2.3, the ITFRSNP system includes only two rule neurons (TIME-type and OR-type) to express the reasoning rules required by the subsequent general fault diagnosis model. This study formulates a set of reasoning algorithms based on matrix calculations to realize iterative reasoning of the fault diagnosis model. The rTSSNPS system requires three types of rule neurons (general neurons, "and" neurons, and "or" neurons) to express the reverse reasoning, comparison, and fusion of temporal constraints and confidence degrees. Additionally, rTSSNPS requires two sets of reasoning algorithms. The first algorithm realizes the reverse reasoning of temporal constraints and comparison of confidence, and the second algorithm fuses the confidence degrees and temporal constraints obtained by the first algorithm. By contrast, the ITFRSNP system uses fewer rule neurons to realize correlation reasoning with confidence and temporal constraints, simplifying the reasoning process and reducing its complexity.

3. ITFRSNP System-Based General Fault Diagnosis Model and Its Fault Diagnosis Process

This section proposes a general fault diagnosis model and its fault diagnosis process based on the ITFRSNP system, to simplify the modeling process of the fault diagnosis. Moreover, a new search method for suspected faulty components is proposed to improve the efficiency of fault diagnosis.

3.1. ITFRSNP System-Based General Fault Diagnosis Model and Fault Diagnosis Principle

The fault diagnosis components include the lines, buses, and transformers. The CBs and relay protection configurations are shown in Figure 2. The bus (B2) is configured with CBs (CB_{bm1} and CB_{bm2}), bus PR (Bm), remote backup PRs (Bs1 and Bs2), and their corresponding CBs (CB_{bs1} and CB_{bs2}). The sending (s) and receiving (r) ends of the line (L2) are equipped with CBs (CB_{lsm} and CB_{lrm}), their associated main PRs (Lsm and Lrm), and near backup PRs (Lsp and Lrp), as well as remote backup PRs (Lss and Lrs) and corresponding CBs (CB_{lss} and CB_{lrs}), respectively. The transformer (T) is equipped with CBs (CB_{tsm} and CB_{trm}), main PR (Tm), near backup PR (Tp), remote backup PRs (Lss and Lrs), and corresponding CBs (CB_{tss} and CB_{trs}).

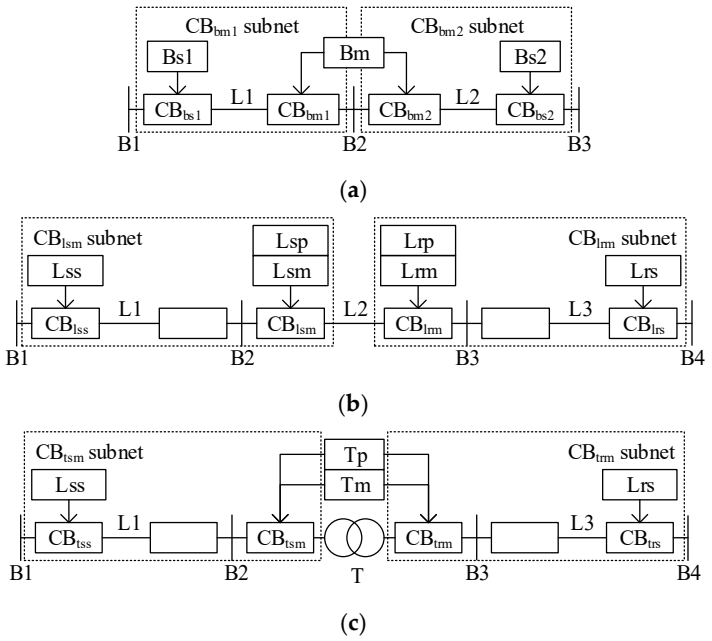


Figure 2. Relay protection configurations of (**a**) bus, (**b**) line, and (**c**) transformer.

As shown in Figure 2, the main and near backup PRs of each CB and the remote backup PRs and their corresponding CBs are configured similarly. Therefore, to conveniently describe the construction principle of the fault diagnosis model, the net consisting of each CB and its main and near backup PRs, as well as the CBs and their remote backup PRs corresponding to the remote end of the adjacent line, can be regarded as a subnet (the subnet is named after the CB is connected to the component, as shown in the dotted box in Figure 2). The PRs and CBs configured for each component can be divided into a corresponding number of subnets, based on the number of connected CBs. For example, the PRs and CBs configured for bus B2 are divided into two subnets of CB_{bm1} and CB_{bm2}.

Each CB subnet consists of a main PR, near-backup PR, remote backup PRs, and their corresponding CBs. The operation logic of the PRs and CBs in each subnet is consistent. The difference between each subnet is the number of remote backup PRs, corresponding CBs, and protection types in the subnet. Based on the commonality and characteristics of subnets, this study constructs an ITFRSNP system-based general fault diagnosis model for the subnet according to the PRs, CBs, and their operation logic. The number of remote backup PRs and corresponding CBs for each component varies owing to the number of neighboring lines. The remote backup PRs and corresponding CBs are preprocessed, and a proposition neuron is used to represent the operational states of all remote backup PRs (corresponding CBs) in the subnet.

The ITFRSNP system-based general fault diagnosis model is shown in Figure 3. σ_{p1}, σ_{p2}, and σ_{p3} record the confidence degrees and time-point constraints of the CBs in the subnet, σ_{p4}, σ_{p5}, and σ_{p6} record the confidence degrees and time-point constraints of the

PRs in the subnet. The corresponding devices are marked below the proposition neurons in the CB and PR layers, respectively. CB_{mPR} and CB_{nPR} represent the CB connected to the components in a subnet. Because the CB has different confidence degrees when corresponding to the main PR or near backup PR (as shown in Table 1), σ_{p1} and σ_{p2} record the confidence degrees when the CB corresponds to the main PR and near the backup PR, respectively. CB_{rPR} and rPR denote the remote CBs of the adjacent lines and the corresponding remote backup PRs in the subnet, respectively. $\sigma_{r1}, \ldots, \sigma_{r6}$ are TIME-type rule neurons that perform reverse reasoning on the time-point constraints of the PRs and CBs. σ_{p7}, σ_{p8}, and σ_{p9} in the middle layer recorded the fusion results of CBs and PRs. σ_{r7} is an OR-type rule neuron that selects the protection type for the fault isolation. σ_{p10} outputs diagnosis results for the subnet.

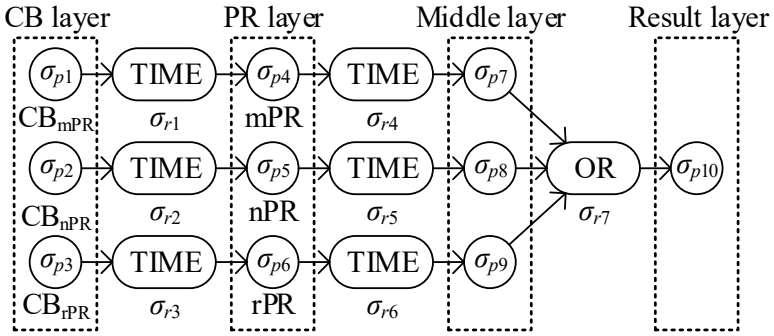


Figure 3. The ITFRSNP system-based general fault diagnosis model.

Table 1. Spike values of PRs and CBs with alarm messages.

Components		Line	Bus	Transformer
Main	PR	0.9913	0.8564	0.7756
	CB	0.9833	0.9833	0.9833
Near backup	PR	0.80	0	0.75
	CB	0.85	0	0.8
Remote backup	PR	0.70	0.70	0.70
	CB	0.75	0.75	0.75

The pretreatment process of remote backup PRs and their corresponding CBs is as follows:

$$\begin{cases} \alpha_{p3} = \frac{n_{\text{CBrPR.o}} \times \varphi_{\text{CBCBrPR.o}} + n_{\text{CBrPR.c}} \times \varphi_{\text{CBrPR.c}}}{n_{\text{CBrPR.o}} + n_{\text{CBrPR.c}}} \\ \alpha_{p6} = \frac{n_{\text{rPR.o}} \times \varphi_{\text{rPR.o}} + n_{\text{rPR.c}} \times \varphi_{\text{rPR.c}}}{n_{\text{rPR.o}} + n_{\text{rPR.c}}} \\ T_{p3} = \bigcup_{i=1}^{\text{CBrPR.o}} T_{\text{CBrPR.o}i} \\ T_{p6} = \bigcup_{i=1}^{n\text{rPR.o}} T_{\text{rPR.o}i} \end{cases} \tag{21}$$

where α_{p3} and T_{p3} are the spike value and time-point constraint of the CB corresponding to the remote backup PR in the subnet, respectively, α_{p6} and T_{p6} are the spike value and time-point constraint of the remote backup PR in the subnet. $n_{\text{CBrPR.o}}$ ($n_{\text{CBrPR.c}}$) is the number of operated (non-operated) CBs corresponding to the remote backup PRs and $n_{\text{rPR.o}}$ ($n_{\text{rPR.c}}$) is the number of operated (non-operated) remote backup PRs. $\varphi_{\text{CBrPR.o}}$ ($\varphi_{\text{CBrPR.c}}$) is the spike value of the operated (non-operated) CB corresponding to the remote backup PR; $\varphi_{\text{rPR.o}}$ ($\varphi_{\text{rPR.c}}$) is the spike value of the operated (non-operated) remote backup PR; $T_{\text{rPR.oi}}$ and $T_{\text{CBrPR.oi}}$ are the time-point constraints for the i-th operated remote backup PR and its corresponding operated CB, respectively.

Combined with Section 2.3, the diagnosis process of the general fault diagnosis model is as follows.

1. σ_{p1}, σ_{p2}, and σ_{p3} fire, and the confidence degrees and time-point constraints of the CBs are input into σ_{r1}, σ_{r2}, and σ_{r3}.
2. σ_{r1}, σ_{r2}, and σ_{r3} infer the time-point constraints of the PRs according to the time-point constraints and time-distance constraints of the CBs. Then, σ_{r1}, σ_{r2}, and σ_{r3} fire, and the confidence degrees of the CBs and the temporal reasoning results of the PRs are input into σ_{p4}, σ_{p5}, and σ_{p6}.
3. σ_{p4}, σ_{p5}, and σ_{p6} fuse the confidence degrees of the PRs and CBs, and the temporal reasoning results from σ_{p4}, σ_{p5}, and σ_{p6} are matched with the time-point constraints of the PRs in σ_{p4}, σ_{p5}, and σ_{p6}. Then, σ_{p4}, σ_{p5}, and σ_{p6} fire, and the confidence fusion results and temporal matching results are input into σ_{r4}, σ_{r5}, and σ_{r6}.
4. σ_{r4}, σ_{r5}, and σ_{r6} infer the fault time based on the temporal matching results and the time-distance constraints of the PRs. Then, σ_{r4}, σ_{r5}, and σ_{r6} fire, and the confidence fusion results and temporal reasoning results of the fault time are input into σ_{p7}, σ_{p8}, and σ_{p9}. Finally, σ_{p7}, σ_{p8}, and σ_{p9} fire, these results are input into σ_{r7}.
5. σ_{r7} is responsible for selecting the highest confidence degree among σ_{p7}, σ_{p8}, and σ_{p9} and its time-point constraints as the diagnosis result of the subnet output into σ_{p10}.

The fault diagnosis results for each subnet can be obtained using a general fault diagnosis model. These diagnosis results of the suspected faulty component can be fused to determine whether the component is faulty. The fault diagnosis principle of the general fault diagnosis model is shown in Figure 4.

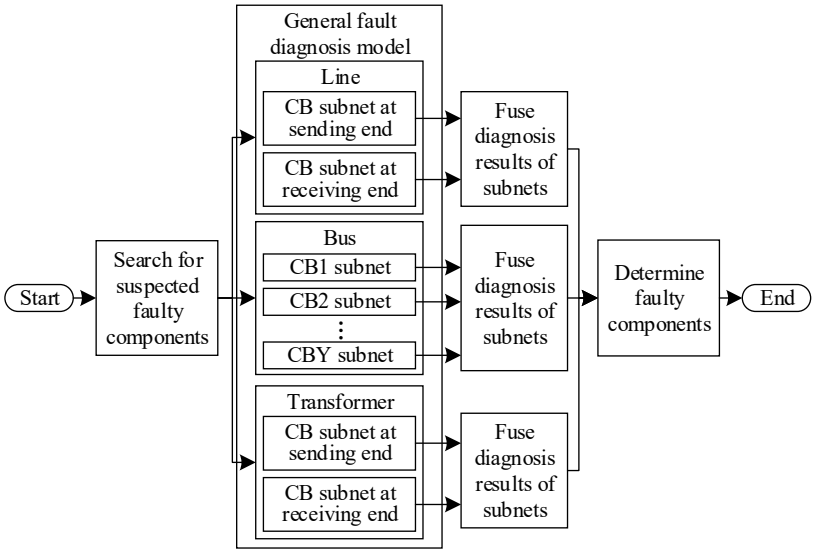


Figure 4. The fault diagnosis principle based on the general fault diagnosis model.

Fault diagnosis models are built based on PRs, CBs, and their operational logic in the existing methods. However, the number of adjacent lines may differ for each component and the numbers of PRs and CBs configured for each component are also different. Therefore, fault diagnosis models for components have different scales and structures, and must be modeled online. Additionally, when the power grid topology changes, the number of PRs and CBs configured for the component changes accordingly. Therefore, it is necessary to adjust or reconstruct a fault diagnosis model to adapt it to a new topology. Existing methods do not propose efficient automatic modeling methods, and their process of constructing and reconstructing fault diagnosis models is complicated for online applications, thereby reducing the efficiency of fault diagnosis. In this study, a general fault diagnosis model is constructed for a CB subnet. Its structure and scale are not affected by the component types, number of remote backup PRs and their corresponding CBs, or topological changes. It is suitable for fault diagnosis of various components with good universality and adaptability.

The fault diagnosis principle simplifies the modeling process and improves the efficiency of fault diagnosis.

3.2. Model Parameters of the General Fault Diagnosis Model

The parameters of the general fault diagnosis model according to the propositions and reasoning rules of the neurons are as follows.

1. The input matrices $\boldsymbol{U}_1$ and $\boldsymbol{U}_2$, and the output matrix $\boldsymbol{V}$ of the general fault diagnosis model are as follows:

$$\boldsymbol{U}_1 = \begin{bmatrix} \boldsymbol{I}_{6\times6} & \boldsymbol{O}_{6\times1} \\ \boldsymbol{O}_{4\times6} & \boldsymbol{O}_{4\times1} \end{bmatrix} \tag{22}$$

$$\boldsymbol{U}_2 = \begin{bmatrix} \boldsymbol{O}_{6\times6} & \boldsymbol{O}_{6\times1} \\ \boldsymbol{O}_{3\times6} & \boldsymbol{E}_{3\times1} \\ \boldsymbol{O}_{1\times6} & \boldsymbol{O}_{1\times1} \end{bmatrix} \tag{23}$$

$$\boldsymbol{V} = \begin{bmatrix} \boldsymbol{O}_{7\times3} & \boldsymbol{I}_{7\times7} \end{bmatrix} \tag{24}$$

   where $\boldsymbol{I}$ is the unit matrix, $\boldsymbol{O}$ is the zero matrix, and $\boldsymbol{E}$ is the matrix with all the elements equal to 1.
2. Considering the uncertainty of the alarm messages, the spike values of PRs and CBs with alarm messages are listed in Table 1, and the spike values of PRs and CBs without alarm messages are 0.2 [21]. The spike values of the proposition and rule neurons in the other layers are 0.
3. If the PR/CB operation time is t_0, the time-point constraint of the related proposition neuron is $[t_0, t_0]$. For PR/CB without an alarm message, the time-point constraint of the related proposition neuron is $\varnothing$.
4. The time-distance constraints for the bus PR, main PR, near backup PR, and remote backup PR are [10, 40] ms, [10, 40] ms, [310, 340] ms, and [510, 540] ms relative to the fault time, respectively. The time-distance constraint for the CB is [20, 40] ms relative to the protection operation time. Therefore, the vector $\boldsymbol{D}_r$ of the general fault diagnosis model is as follows:

$$\boldsymbol{D}_r = [[20,40],[20,40],[20,40],[10,40],[310,340],[510,540],\varnothing]^{\mathrm{T}} \tag{25}$$

5. The spike numbers of the proposition neurons in the PR and CB layers are set to 1, and the spike numbers of the other neurons are set to zero to ensure that spikes from proposition neurons can be delivered to rule neurons. Therefore, the vectors $\boldsymbol{\theta}_p$ and $\boldsymbol{\theta}_r$ of the general fault diagnosis model are as follows:

$$\begin{cases} \boldsymbol{\theta}_p = [1,1,1,1,1,1,0,0,0,0]^T \\ \boldsymbol{\theta}_r = [0,0,0,0,0,0,0]^T \end{cases} \tag{26}$$

6. Because the PR layer neurons need to obtain spikes from the CB layer neurons to fire, the spike number thresholds of all proposition neurons in the PR layer are set to two, and the spike number thresholds of other proposition neurons are set to one. Rule neurons must obtain spikes from all input proposition neurons to fire; therefore, their spike number thresholds are equal to the number of their input proposition neurons. Therefore, the vectors $\boldsymbol{\lambda_p}$ and $\boldsymbol{\lambda_r}$ of the general fault diagnosis model are as follows:

$$\begin{cases} \boldsymbol{\lambda}_p = [1,1,1,2,2,2,1,1,1,1]^{\mathrm{T}} \\ \boldsymbol{\lambda}_r = [1,1,1,1,1,1,3]^{\mathrm{T}} \end{cases} \tag{27}$$

3.3. ITFRSNP System-Based General Fault Diagnosis Process

3.3.1. Suspected Faulty Component Search Method

As mentioned in the introduction, the missing alarm message from the CB at the boundary of the outage area (referred to as the boundary CB) significantly affects the diagnosis efficiency. A missing boundary CB alarm can result in outage areas not being recognized. All components in the power system are diagnosed to identify faulty components. In practical applications, it is difficult to traverse the entire power system topology and construct fault diagnosis models for all the components, and the workload is large. Therefore, this study proposes a new search method for suspected faulty components. According to the relay protection configuration, when a fault occurs in a component, the main PR trips the CBs to isolate the faulty component; if the CB refuses to trip, the backup protection at the remote end of the neighboring component trips the corresponding CB. It illustrates that the faults of the components connected and adjacent to the CB cause the CB to trip. Therefore, this study searches for components connected and adjacent to the tripped CBs as their isolation ranges; the isolation ranges of different CBs take the intersection of two to determine the suspected faulty components, thus narrowing down the scope of fault diagnosis.

The specific steps to search for suspected faulty components are as follows.

1. Alarm messages are received from the W CBs. These CBs form the CB set (*CBS*). Initialize $w = 1$ and begin the search.
2. Select the w-th CB (CB_w) in *CBS*.
3. Buses, lines, and transformers connected to CB_w are searched to form the w-th subset of suspected faulty components (COM_w).
4. Adjacent buses, lines and transformers are searched in the direction of the line or transformer connected to the CB_w and placed into COM_w.
5. If $w = W$, proceed to the next step; otherwise, $w = w + 1$ and return to Step 3.
6. The suspected faulty component subsets intersect in pairs. If the intersection of two suspected faulty components is not empty, then the intersection results are combined into a total set of suspected faulty components (*COMS*). If the intersection of a certain suspected faulty component subset with other subsets is empty, all the components in this subset are input into *COMS*. The components in *COMS* are suspected to be faulty components.

3.3.2. Fault Diagnosis Process

The suspected fault component search method is used to determine the diagnosis range, and then the fault diagnosis is performed individually for the subnets of the suspected faulty components. Finally, the diagnosis results of each subnet are fused to determine the faulty components. The specific fault diagnosis process used in this study is as follows.

1. After receiving the alarm messages, start the search method for suspected faulty components and set the total number of suspected faulty components as X. Initialize $x = 1$.
2. Select the x-th suspected faulty component and set the number of CBs connected to it as Y. Initialize $y = 1$.
3. Initialize the general fault diagnosis model with neuron spike values of zero and time-point constraints of $\varnothing$. The y-th CB is selected for search. If the x-th suspected faulty component is a line or transformer, search for the main PR and near-backup PR corresponding to the CB. If the x-th suspected faulty component is a bus, the bus PR corresponding to the CB is searched. According to the alarm messages, σ_{p1}, σ_{p2}, σ_{p4}, and σ_{p5} in the general fault diagnosis model are assigned spike values and time-point constraints concerning Section 3.1.
4. The number of adjacent lines of the y-th CB is set as Z. If Z = 0, skip to Step 8; otherwise, initialize $z = 1$.

5. The initial values of $n_{\mathrm{CBrPR.o}}$, $n_{\mathrm{CBrPR.c}}$, $n_{\mathrm{rPR.o}}$, and $n_{\mathrm{rPR.c}}$ are 0; the initial values of $T_{\mathrm{CBrPR.oi}}$ and $T_{\mathrm{rPR.oi}}$ are ∅. Search for CBs at the far end of the z-th adjacent line. If the CB has an alarm message at t_{CBrPRz}, then $n_{\mathrm{CBrPR.o}} = n_{\mathrm{CBrPR.o}} + 1$, and $T_{\mathrm{CBrPR}} = T_{\mathrm{CBrPR}} \cup [t_{\mathrm{CBrPRz}}, t_{\mathrm{CBrPRz}}]$; otherwise, $n_{\mathrm{CBrPR.c}} = n_{\mathrm{CBrPR.c}} + 1$. Search for the remote backup PR corresponding to the CB at the far end of the z-th adjacent line, and if this remote backup PR has an alarm message at t_{rPRz}, then $n_{\mathrm{rPR.o}} = n_{\mathrm{rPR.o}} + 1$ and $T_{\mathrm{rPR}} = T_{\mathrm{rPR}} \cup [t_{\mathrm{rPRz}}, t_{\mathrm{rPRz}}]$; otherwise, $n_{\mathrm{rPR.c}} = n_{\mathrm{rPR.c}} + 1$.
6. If $z < \mathrm{Z}$, $z = z + 1$, and return to Step 5; otherwise, substitute $n_{\mathrm{CBrPR.o}}$, $n_{\mathrm{CBrPR.c}}$, $n_{\mathrm{rPR.o}}$, $n_{\mathrm{rPR.c}}$, T_{CBrPR}, and T_{rPR} into (21) to yield α_{p3}, T_{p3}, α_{p6}, and T_{p6}.
7. Based on the parameter definitions in Section 2.3, the inputs ($\alpha^0_{p(xy)}$ and $T^0_{p(xy)}$) are determined for the general fault diagnosis model corresponding to the y-th CB subnet of the x-th suspected faulty component. The reasoning algorithm in Section 2.3 is introduced to obtain the diagnosis result ($\alpha_{p10(xy)}$ and $T_{p10(xy)}$ of σ_{p10}) for the y-th CB subnet.
8. If $y < \mathrm{Y}$, then $y = y + 1$ and return to Step 3; otherwise, the diagnosis results ($\alpha_{(x)}$ and $T_{(x)}$) of the x-th suspected faulty component are obtained by substituting the diagnosis results of the subnets of this component into the following equations:

$$\begin{cases} \alpha(x) = \underset{y=1}{\overset{\mathrm{Y}}{avg}}(\alpha p10(xy)) \\ T(x) = \underset{y=1}{\overset{\mathrm{Y}}{\cap}}(\alpha p10(xy)) \end{cases} \tag{28}$$

9. The measured value $\eta_{(x)}$ of the x-th suspected faulty component is obtained by substituting $\alpha_{(x)}$ and $T_{(x)}$ into the measurement function, as shown in Equation (29). The threshold of the measured value was set to 0.6, considering the uncertainty and timestamp errors of the alarm messages. A component is faulty if $\eta_{(x)}$ is greater than 0.6.

$$\begin{cases} R(T(x)) = \begin{cases} 1, & T(a) \neq \varnothing \\ 0, & other \end{cases} \\ \eta(x) = 0.7\alpha(x) + 0.3R(T(x)) \end{cases} \tag{29}$$

10. If $x < \mathrm{X}$, then $x = x + 1$ and return to Step 2; otherwise, complete the fault diagnosis for all suspected faulty components and end the fault diagnosis process.

4. Case Studies

In this section, the IEEE-39 bus power system (as shown in Figure 5) is used to simulate the fault cases and verify the effectiveness and reliability of the proposed method. These cases include single faults, double faults, PR/CB rejections, missing alarm messages, and error timestamps. They prove that the proposed method can ensure the accuracy and fault tolerance of the diagnosis results for complex faults.

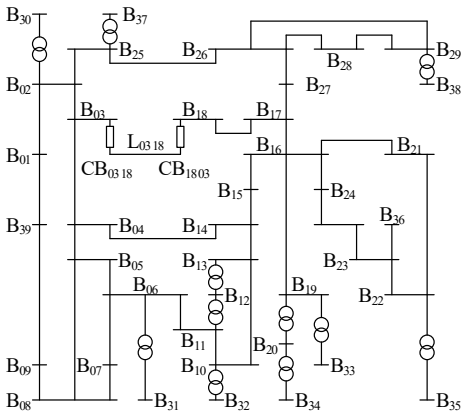


Figure 5. IEEE 39-bus power system.

In Figure 5, B denotes buses, L denotes lines, T denotes transformers, Lp denotes line PR, Bp denotes bus PR, Tp denotes transformer PR, and the subscripts m, p, and s indicate the main, near backup, and remote backup PRs, respectively. For example, the line connecting B_{03} and B_{18} is L_{0318}; the transformer connecting B_{02} and B_{30} is T_{0230}; the CB of L_{0318} near B_{03} is CB_{0318}; the CB near B_{18} is CB_{1803}; Lp_{0318}m, Lp_{0318}p, and Lp_{0318}s indicate the main, near backup, and remote backup PRs configured by CB_{0318}; Bp_{03} is the bus PR configured by B_{03}; and Tp_{0230}m and Tp_{0230}p are the main and near backup PRs configured by T_{0230}.

4.1. Fault Case Analysis

4.1.1. Case 1 (Bus Fault)

Considering Figure 5 as an example, a fault occurs at B_{18}. Bp_{18} operates, and then CB_{1817} and CB_{1803} trip. The alarm messages are briefly described as $Bp_{18}(0)$, $CB_{1817}(35)$, and $CB_{1803}(40)$, where the brackets are the operation times, the first alarm message is the zero moment, and the unit is ms. The fault diagnosis process is as follows:

1. CBS = {CB_{1817}, CB_{1803}} can be obtained from the alarm message. Traverse CBS and search for suspected faulty components. There are a subset COM_{1817} = {B_{18}, L_{1817}, B_{17}, L_{1727}, L_{1617}}, a subset COM_{1803} = {B_{18}, L_{0318}, B_{03}, L_{0203}, L_{0304}}, and a total set $COMS$ = {B_{18}}.
2. B_{18} is selected for fault diagnosis. CB_{1803} connected to B_{18} is selected for the search, and its corresponding bus PR is Bp_{18}, respectively. According to the alarm messages, the spike values of σ_{p1}, σ_{p2}, σ_{p4}, and σ_{p5} are 0.9833, 0.85, 0.8564, and 0, respectively, and their time-point constraints are [40, 40], [40, 40], [0, 0], and $\varnothing$, respectively.
3. The adjacent line corresponding to CB_{0318} is L_{0318}, the CB at the far end is CB_{0318}, and the remote backup PR is Lp_{0318}s. Because the alarm information is not received from the above PRs and CBs, $n_{\mathrm{CBrPR.o}} = 0$, $n_{\mathrm{CBrPR.c}} = 1$, $T_{\mathrm{CBrPR}} = \varnothing$, $n_{\mathrm{rPR.o}} = 0$, $n_{\mathrm{rPR.c}} = 1$, and $T_{\mathrm{rPR}} = \varnothing$. Substituting them into (21) to obtain the spike values and time-point constraints for σ_{p3} and σ_{p6} are 0.2 and $\varnothing$, respectively.
4. $\alpha^0_{p(11)}$ and $T^0_{p(11)}$ of the fault diagnosis model for the CB_{1803} subnet are as follows:

$$\begin{cases} \boldsymbol{\alpha}^0_{p(11)} = [0.9833, 0.85, 0.2, 0.8564, 0, 0.2, 0, 0, 0, 0]^{\mathrm{T}} \\ \boldsymbol{T}^0_{p(11)} = [[40, 40], [40, 40], \varnothing, [0, 0], \varnothing, \varnothing, \varnothing, \varnothing, \varnothing, \varnothing]^{\mathrm{T}} \end{cases} \tag{30}$$

5. $\boldsymbol{\alpha}^0_{p(11)}$, $\boldsymbol{T}^0_{p(11)}$ and model parameters are imported into the reasoning algorithm, the diagnosis results of the CB_{1803} subnet are $\alpha_{p10(11)} = 0.9199$, $T_{p10(11)} = [-40, -10]$.
6. Similarly, $\boldsymbol{\alpha}^0_{p(12)}$ and $\boldsymbol{T}^0_{p(11)}$ of the fault diagnosis model for the CB_{1817} subnet are as follows:

$$\begin{cases} \boldsymbol{\alpha}^0_{p(12)} = [0.9833, 0.85, 0.2, 0.8564, 0, 0.2, 0, 0, 0, 0]^{\mathrm{T}} \\ \boldsymbol{T}^0_{p(12)} = [[35, 35], [35, 35], \varnothing, [0, 0], \varnothing, \varnothing, \varnothing, \varnothing, \varnothing, \varnothing]^{\mathrm{T}} \end{cases} \tag{31}$$

7. Similarly, the diagnosis results for the CB_{1817} subnet are $\alpha_{p10(12)} = 0.9199$ and $T_{p10(12)} = [-40, -10]$.
8. $\alpha_{p10(11)}$, $T_{p10(11)}$, $\alpha_{p10(12)}$ and $T_{p10(12)}$ are substituted into (28), and the diagnosis results $\alpha_{(1)} = 0.9199$ and $T_{(1)} = [-40, -10]$ for B_{18}. $\alpha_{(1)}$ and $T_{(1)}$ are substituted into (29), and the measured value of B_{18} is $\eta_{(1)} = 0.9439$, which is greater than 0.6. Therefore, B_{18} is a faulty component.

This case demonstrates that the proposed method can diagnose bus faults and their corresponding time-point constraints.

4.1.2. Case 2 (Line Fault with the CB Rejection)

Considering Figure 5 as an example, a fault occurs at L_{0318}. Lp_{0318}m and Lp_{1803}m operate, and then CB_{0318} trips, but CB_{1803} fails to operate; thus, Lp_{1718}s operates and CB_{1718}

trips. The alarm messages are briefly described as $Lp_{1803}m(0)$, $Lp_{0318}m(2)$, $CB_{0318}(30)$, $Lp_{1718}s(520)$, and $CB_{1718}(541)$. The fault diagnosis process is as follows.

1. Based on the alarm messages, *COMS* = {L_{0318}, L_{1718}, B_{18}} is obtained.
2. L_{0318} is selected for fault diagnosis. The $\boldsymbol{\alpha}^0_{p(11)}$, $\boldsymbol{T}^0_{p(11)}$, $\boldsymbol{\alpha}^0_{p(12)}$, and $\boldsymbol{T}^0_{p(12)}$ of the fault diagnosis model for the CB_{0318} and CB_{1803} subnets are as follows.

$$\begin{cases} \boldsymbol{\alpha}^0_{p(11)} = [0.9833, 0.85, 0.2, 0.9913, 0.2, 0.2, 0, 0, 0, 0]^{\mathrm{T}} \\ \boldsymbol{T}^0_{p(11)} = [[30, 30], [30, 30], \varnothing, [2, 2], \varnothing, \varnothing, \varnothing, \varnothing, \varnothing, \varnothing]^{\mathrm{T}} \end{cases} \tag{32}$$

$$\begin{cases} \boldsymbol{\alpha}^0_{p(12)} = [0.2, 0.2, 0.75, 0.9913, 0.2, 0.7, 0, 0, 0, 0]^{\mathrm{T}} \\ \boldsymbol{T}^0_{p(12)} = [\varnothing, \varnothing, [541, 541], [0, 0], \varnothing, [520, 520], \varnothing, \varnothing, \varnothing, \varnothing]^{\mathrm{T}} \end{cases} \tag{33}$$

3. The diagnosis results for the CB_{0318} subnet are $\alpha_{p10(11)} = 0.9873$ and $T_{p10(11)} = [-38, -8]$. The diagnosis results of the CB_{1803} subnet are $\alpha_{p10(12)} = 0.725$ and $T_{p10(12)} = [-20, 10]$. The diagnosis results of L_{0318} are $\alpha_{(1)} = 0.8562$ and $T_{(1)} = [-20, 10]$, and its measured value is $\eta_{(1)} = 0.8993$, which is greater than 0.6. Thus, L_{0318} is a faulty component.
4. Similarly, the measured values of L_{1718} and B_{18} are 0.3733 and 0.42, respectively, and L_{1718} and B_{18} are non-faulty components.

CB_{1803} refused to operate in this case, and the suspected faulty component extended to L_{1718} and B_{18}. However, the proposed method is not misdiagnosed, and its diagnosis results are accurate. This case proves that the method in this study can diagnose a faulty line with CB rejection and non-faulty components.

4.1.3. Case 3 (Transformer Fault with Missing CB Alarm Message)

Considering Figure 5 as an example, a fault occurs at T_{1213}. $Tp_{1213}m$ operates, and then CB_{1213} and CB_{1312} trip. However, the alarm message for CB_{1312} is lost. The alarm messages are briefly described as $Tp_{1213}m(0)$ and $CB_{1213}(32)$. The fault diagnosis process is as follows:

1. Based on the alarm messages, *COMS* = {T_{1213}, B_{12}, B_{13}, L_{1314}, L_{1013}} is obtained.
2. T_{1213} is selected for fault diagnosis. The $\boldsymbol{\alpha}^0_{p(11)}$, $\boldsymbol{T}^0_{p(11)}$, $\boldsymbol{\alpha}^0_{p(12)}$, and $\boldsymbol{T}^0_{p(12)}$ of the fault diagnosis model for the CB_{1312} and CB_{1213} subnets are as follows.

$$\begin{cases} \boldsymbol{\alpha}^0_{p(11)} = [0.2, 0.2, 0.2, 0.7756, 0.2, 0.2, 0, 0, 0, 0]^{\mathrm{T}} \\ \boldsymbol{T}^0_{p(11)} = [\varnothing, \varnothing, \varnothing, [0, 0], \varnothing, \varnothing, \varnothing, \varnothing, \varnothing, \varnothing]^{\mathrm{T}} \end{cases} \tag{34}$$

$$\begin{cases} \boldsymbol{\alpha}^0_{p(12)} = [0.9833, 0.8, 0.2, 0.7756, 0.2, 0.2, 0, 0, 0, 0]^{\mathrm{T}} \\ \boldsymbol{T}^0_{p(12)} = [[32, 32], [32, 32], \varnothing, [0, 0], \varnothing, \varnothing, \varnothing, \varnothing, \varnothing, \varnothing]^{\mathrm{T}} \end{cases} \tag{35}$$

3. The diagnosis results for the CB_{1312} subnet are $\alpha_{p10(11)} = 0.4878$ and $T_{p10(11)} = [-40, -10]$. The diagnosis results of the CB_{1213} subnet are $\alpha_{p10(12)} = 0.8795$ and $T_{p10(12)} = [-40, -10]$. The diagnosis results of T_{1213} are $\alpha_{(1)} = 0.6836$ and $T_{(1)} = [-40, -10]$, and its measured value $\eta_{(1)} = 0.7785$, which is greater than 0.6. Thus, T_{1213} is a faulty component.
4. Similarly, the measured values of B_{12}, B_{13}, L_{1314}, and L_{1013} are 0.2771, 0.2042, 0.1881, and 0.1881, respectively, and they are non-faulty components.

In this case, CB_{1312} is a boundary CB, and its alarm message is lost. However, it was not possible to confirm the outage area. The suspected fault component search method searches for T_{1213}, B_{12}, B_{13}, L_{1314}, and L_{1013} within the protection range of CB_{1213}. This search method avoids fault diagnosis in the entire power system. This improves the fault diagnosis efficiency when an alarm message from the boundary CB is lost.

4.1.4. More Cases

More fault cases are presented to demonstrate the accuracy and fault tolerance of the proposed method, and the fault diagnosis results are presented in Table 2. Since the reasoning processes in these cases are consistent with the above cases, their specific reasoning processes are not provided.

Table 2. Fault diagnosis results of more cases.

No.	Fault Descriptions	Brief Descriptions	Suspected Faulty Components	Spike Values	Time-Point Constraints	Measured Values	Faulty Components
4	The fault occurs on B_{18}, and the alarm message of CB_{0318} is missing.	$Bp_{18}(0)$, $CB_{1817}(29)$	B_{18} B_{17} L_{1718} L_{1727} L_{1617}	0.7240 0.2917 0.3958 0.2688 0.2688	$[-40, -20]$ ∅ ∅ ∅ ∅	0.8068 0.2042 0.2771 0.1881 0.1881	B_{18}
5	A fault occurs on B_{18}, CB_{1803} fails to trip, $Lp_{0318}s$ operates, and CB_{0318} trips.	$Bp_{18}(0)$, $CB_{1718}(29)$, $Lp_{0318}s(520)$, $CB_{0318}(540)$	B_{18} L_{1718}	0.8549 0.5625	$[-20, -10]$ ∅	0.8757 0.3938	B_{18}
6	A fault occurs on B_{03}, and the alarm on Bp_{03} is missing.	$CB_{0302}(29)$, $CB_{0304}(31)$, $CB_{0318}(32)$	B_{03}	0.5917	$[-48, -1]$	0.7142	B_{03}
7	A fault occurs on B_{03}, Bp_{03} fails to operate, and remote backup PRs operate.	$Lp_{1803}s(0)$, $Lp_{0403}s(2)$, $Lp_{0203}s(6)$, $CB_{1803}(32)$, $CB_{0403}(35)$, $CB_{0203}(36)$	B_{03} L_{0203} L_{0304} L_{0318}	0.725 0.6583 0.6583 0.6583	$[-534, -510]$ ∅ ∅ ∅	0.8075 0.4608 0.4608 0.4608	B_{03}
8	A fault occurs on L_{0318}, $Lp_{1803}m$ fails to operate, and $Lp_{1803}p$ operates, but the timestamp of $Lp_{1803}p$ is incorrect.	$Lp_{0318}m(0)$, $CB_{0318}(30)$, $Lp_{1803}p(200)$, $CB_{1803}(325)$	L_{0318}	0.9062	$[-40, -5]$	0.9343	L_{0318}
9	A fault occurs on L_{0318}, CB_{1803} fails to trip, and the alarm message of $Lp_{0318}m$ is missing.	$Lp_{1803}m(0)$, $CB_{0318}(25)$, $Lp_{1718}s(500)$, $CB_{1718}(515)$	L_{0318} L_{1718} B_{18}	0.6583 0.5333 0.6	$[-40, -10]$ ∅ ∅	0.7608 0.3733 0.42	L_{0318}
10	A fault occurs on L_{0318}, CB_{1803} fails to trip, and the alarm message of CB_{0318} is missing.	$Lp_{0318}m(0)$, $Lp_{1803}m(5)$, $Lp_{1718}s(500)$, $CB_{1718}(515)$	L_{0318} L_{1718} B_{18} B_{17}	0.6603 0.3958 0.4625 0.3958	$[-35, -10]$ ∅ ∅ ∅	0.7622 0.2771 0.3238 0.2771	L_{0318}
11	A fault occurs on T_{1213} and the alarm message of CB_{1312} is missing.	$Tp_{1213}m(0)$, $CB_{1213}(5)$	T_{1213} B_{12} B_{13} L_{1314} L_{1013}	0.6836 0.3958 0.2917 0.2688 0.2688	$[-40, -10]$ ∅ ∅ ∅ ∅	0.7785 0.2771 0.2042 0.1881 0.1881	T_{1213}
12	A fault occurs on T_{1213}, CB_{1803} fails to trip, Lp_{1413} and $Lp_{1013}s$ operate, and CB_{1413} and CB_{1013} trip.	$Tp_{1213}m(0)$, $CB_{1213}(32)$, $Lp_{1413}s(525)$, $Lp_{1013}s(530)$, $CB_{1413}(540)$, $CB_{1013}(545)$	T_{1213} B_{13} L_{1314} L_{1013}	0.8224 0.475 0.5333 0.5333	$[-15, -10]$ ∅ ∅ ∅	0.8757 0.3325 0.3733 0.3733	T_{1213}
13	A fault occurs on L_{0318}, the alarm message of CB_{0318} is missing. A fault occurs on L_{1718}.	$Lp_{0318}m(0)$, $Lp_{1803}m(5)$, $CB_{1803}(35)$, $Lp_{1817}m(120)$, $Lp_{1718}m(128)$, $CB_{1817}(145)$, $CB_{1718}(153)$	L_{0318} L_{1718} B_{17} B_{18}	0.7915 0.9873 0.3306 0.5917	$[-35, -10]$ [88, 110] ∅ ∅	0.8540 0.9911 0.2314 0.4142	L_{0318} L_{1718}

Table 2. *Cont.*

No.	Fault Descriptions	Brief Descriptions	Suspected Faulty Components	Spike Values	Time-Point Constraints	Measured Values	Faulty Components
14	A fault occurs on L_{0318}, and CB_{1803} fails to trip. A fault occurs on B_{17}.	$Lp_{1803}m(0)$, $Lp_{0318}m(2)$, $CB_{0318}(30)$, $Lp_{1718}s(520)$, $CB_{1718}(541)$, $Bp_{17}(100)$, $CB_{1727}(135)$, $CB_{1716}(140)$,	L_{0318}	0.8562	$[-20, 10]$	0.8993	L_{0318} B_{17}
			L_{1718}	0.5333	∅	0.3733	
			B_{17}	0.9199	[60, 80]	0.9493	
			B_{18}	0.6	∅	0.42	
15	A fault occurs on B_{03}, the alarm message of CB_{0318} is missing. A fault occurs on B_{03}, but the timestamp of CB_{1415} is incorrect.	$Bp_{03}(0)$, $CB_{0302}(29)$, $CB_{0304}(31)$, $Bp_{14}(250)$, $CB_{1404}(275)$, $CB_{1415}(284)$, $CB_{1413}(385)$	B_{03}	0.8549	$[-27, -10]$	0.8984	B_{03} B_{14}
			B_{14}	0.9199	[210, 240]	0.9493	
16	A fault occurs on B_{18}, Bp_{18} fails to operate, and remote backup PRs operate. A fault occurs on T_{1213}, and the alarm on Bp_{11} is missing; a fault occurs on L_{0204}.	$Lp_{0318}s(0)$, $Lp_{1718}s(5)$, $CB_{0318}(32)$, $CB_{1718}(35)$ $CB_{1312}(50)$, $CB_{1213}(60)$	B_{18}	0.725	$[-534, -510]$	0.8075	B_{18} T_{1213}
			L_{0318}	0.6583	∅	0.4608	
			L_{1718}	0.6583	∅	0.4608	
			T_{1213}	0.5917	$[-20, 20]$	0.7142	
			B_{12}	0.3958	∅	0.2771	
			B_{13}	0.3306	∅	0.2314	

Cases 4 and 5 are based on Case 1, simulating the missing alarm message and rejection of CBs. Although the number of suspected faulty components and spike values of non-faulty components increased, the proposed method still accurately diagnoses the faulty bus.

Cases 6 and 7 are bus faults with missing alarm messages and rejection of the bus PR. If the spike value is the diagnosis basis and its threshold is set to 0.6, B_{03} will be diagnosed as a non-faulty component in Case 6, and the lines adjacent to B_{03} will be misdiagnosed as fault components in Case 7. Because the bus PR is related to multiple CBs and remote backup PRs, the missing alarm message and maloperation of the bus PR significantly affect the diagnosis results of the faulty bus and adjacent non-faulty components. In this case, the proposed method can still diagnose a faulty bus without missed diagnosis and misdiagnosis.

In Case 9, the CB refused to operate, the main PR alarm message was lost, and the spike values of L_{1718} and B_{18} are 0.5333 and 0.6, respectively, which are close to the threshold. Because the fault times of L_{1718} and B_{18} cannot be inferred, L_{1718} and B_{18} are independent of the operating PR and CB and are not faulty components. The main PR configuration of the transformer is similar to that of the bus, whereas that of the remote backup PR configuration is similar to that of the line. Therefore, when the CB alarm message is lost (Case 11), the diagnosis results of the suspected faulty components are similar to those in Case 4 (bus fault with a missing CB alarm message). When the CB refuses to operate, and the backup PR is initiated (Case 12), the diagnosis results of the suspected faulty components are similar to those in Case 12 (line fault with CB rejection). Cases 8–12 prove that the proposed method can accurately diagnose faulty lines and transformers in complex fault scenarios.

Compared with the single faults in the above fault cases, the adjacent faulty components in the double faults (Cases 13–16) have a greater impact on the non-faulty components. For example, the confidence degrees of B_{18} in Case 13, L_{1718} in Case 14, and L_{0318} and L_{1718} in Case 16 are close to or even exceeded the threshold. In Case 16, because the main PR of the transformer is associated with multiple CBs, the loss of the main PR alarm message causes the spike value of the faulty transformer to be lower than 0.6. The diagnosis results of Cases 12–16 are still accurate because of the measured values as the diagnosis basis, which proves that the proposed method still has high accuracy and fault tolerance for double faults.

It is found that the timestamp error of alarm messages (Cases 8 and 15) and adjacent component faults (Cases 13 and 14) affect temporal reasoning. The former is because the wrong time-point constraint cannot satisfy the time-distance constraint. The latter is because the CB time-point constraint cannot satisfy the time-distance constraints for all corresponding PRs. The proposed method can complete temporal reasoning by simultaneously performing reverse reasoning on the CBs and PRs. When the PR or CB in a subnet satisfies the temporal constraint, the temporal reasoning proceeds normally. Moreover, the merged reasoning between subnets can mutually verify whether the temporal reasoning results of the subnets are correct. Therefore, PR/CB maloperation/rejection, timestamp errors, and complex faults have little effect on the temporal reasoning of this method, and the accuracy and fault tolerance of the diagnosis results are not reduced.

The fault diagnosis method based on the ITFRSNP system simultaneously accomplishes temporal and confidence reasoning. The results of temporal and confidence reasoning are quantized using the measurement function, and the results of confidence inference are corrected using temporal reasoning. The proposed method can diagnose faulty components and fault times with high accuracy and fault tolerance in complex fault scenarios, such as single faults, multiple faults, PR/CB rejection, missing alarm messages, and timestamp errors. The fault diagnosis model and reasoning method have good generality and can be applied to the fault diagnosis of buses, lines, and transformers.

4.2. Actual Case Analysis

This study verifies the effectiveness of the proposed fault diagnosis model and diagnosis process with actual fault cases from a city power system in Shandong Province, 2020. The wiring diagram of the power system associated with the fault case is shown in Figure 6. It contains seven substations, nine buses, twenty-one lines, and two transformers.

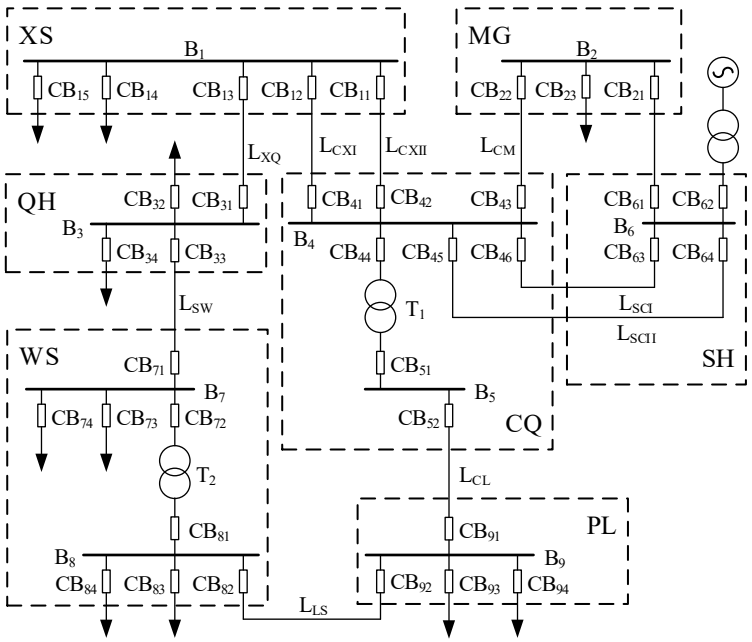


Figure 6. The wiring diagram of the power system.

4.2.1. Case 1

A fault occurs at L_{SW}. $Lp_{71}m$ and $Lp_{33}m$ operate, and then CB_{71} and CB_{33} trip. However, the alarm message for CB_{33} is lost. The alarm messages are briefly described as $Lp_{71}m(0)$, $Lp_{33}m(5)$ and $CB_{71}(25)$. The fault diagnosis process is as follows:

1. *CBS* = {CB_{71}} can be obtained from the alarm message. Traverse *CBS* and search for suspected faulty components. There are a subset COM_{71} = {L_{SW}, L_{XQ}, B_3, B_7}, and a total set *COMS* = {L_{SW}, L_{XQ}, B_3, B_7}.

2. L_{SW} is selected for fault diagnosis. The $\boldsymbol{\alpha}^0_{p(11)}$, $\boldsymbol{T}^0_{p(11)}$, $\boldsymbol{\alpha}^0_{p(12)}$, and $\boldsymbol{T}^0_{p(12)}$ of the fault diagnosis model for the $CB_{71}$and CB_{33} subnets are as follows.

$$\begin{cases} \boldsymbol{\alpha}^0_{p(11)} = [0.9833, 0.2, 0.2, 0.9913, 0.2, 0.2, 0, 0, 0, 0]^{\mathrm{T}} \\ \boldsymbol{T}^0_{p(11)} = [[25, 25], [25, 25], \varnothing, [0, 0], \varnothing, \varnothing, \varnothing, \varnothing, \varnothing, \varnothing]^{\mathrm{T}} \end{cases} \tag{36}$$

$$\begin{cases} \boldsymbol{\alpha}^0_{\mathrm{p}(12)} = [0.2, 0.2, 0.2, 0.9913, 0.2, 0.2, 0, 0, 0, 0]^{\mathrm{T}} \\ \boldsymbol{T}^0_{p(12)} = [\varnothing, \varnothing, \varnothing, [5, 5], \varnothing, \varnothing, \varnothing, \varnothing, \varnothing, \varnothing]^{\mathrm{T}} \end{cases} \tag{37}$$

3. The diagnosis results for the CB_{71} subnet are $\alpha_{p10(11)} = 0.9873$ and $T_{p10(11)} = [-40, -10]$. The diagnosis results of the CB_{33} subnet are $\alpha_{p10(12)} = 0.5567$ and $T_{p10(12)} = [-35, -5]$. The diagnosis results of L_{SW} are $\alpha_{(1)} = 0.7915$ and $T_{(1)} = [-35, -10]$, and its measured value $\eta_{(1)} = 0.8540$, which is greater than 0.6. Thus, T_{1213} is a faulty component.
4. Similarly, the measured values of L_{XQ}, B_3 and B_7 are 0.2363, 0.14, and 0.2085, respectively, and they are non-faulty components.

4.2.2. Case 2

A fault occurs at B_5. Bp_5 operates, and then CB_{51} trips, but CB_{53} fails to operate; thus, Lp_{91}s operates and CB_{91} trips. The alarm messages are briefly described as $Bp_5(0)$, $CB_{51}(29)$, $Lp_{91}s(525)$, and $CB_{91}(550)$. The fault diagnosis process is as follows:

1. *CBS* = {CB_{51}, CB_{91}} can be obtained from the alarm message. Traverse *CBS* and search for suspected faulty components. There are a subset COM_{51} = {B_5, T_1, B_4, L_{CXI}, B_{CXII}, L_{CM}, L_{SCI}, L_{SCII}}, a subset COM_{91} = {B_9, L_{CL}, B_5, T_1}, and a total set *COMS* = {B_5, T_1}.
2. B_5 is selected for fault diagnosis. The $\boldsymbol{\alpha}^0_{p(11)}$, $\boldsymbol{T}^0_{p(11)}$, $\boldsymbol{\alpha}^0_{p(12)}$, and $\boldsymbol{T}^0_{p(12)}$ of the fault diagnosis model for the CB_{51} and CB_{52} subnets are as follows.

$$\begin{cases} \boldsymbol{\alpha}^0_{p(11)} = [0.9833, 0.2, 0.2, 0.8564, 0.2, 0.2, 0, 0, 0, 0]^{\mathrm{T}} \\ \boldsymbol{T}^0_{p(11)} = [[29, 29], [29, 29], \varnothing, [0, 0], \varnothing, \varnothing, \varnothing, \varnothing, \varnothing, \varnothing]^{\mathrm{T}} \end{cases} \tag{38}$$

$$\begin{cases} \boldsymbol{\alpha}^0_{p(12)} = [0.2, 0.2, 0.75, 0.9913, 0.2, 0.7, 0, 0, 0, 0]^{\mathrm{T}} \\ \boldsymbol{T}^0_{p(12)} = [\varnothing, \varnothing, [550, 550], [0, 0], \varnothing, [525, 525], \varnothing, \varnothing, \varnothing, \varnothing]^{\mathrm{T}} \end{cases} \tag{39}$$

3. The diagnosis results for the CB_{51} subnet are $\alpha_{p10(11)} = 0.9873$ and $T_{p10(11)} = [-40, -10]$. The diagnosis results of the CB_{52} subnet are $\alpha_{p10(12)} = 0.5567$ and $T_{p10(12)} = [-15, 15]$. The diagnosis results of B_5 are $\alpha_{(1)} = 0.7915$ and $T_{(1)} = [-15, -10]$, and its measured value $\eta_{(1)} = 0.8540$, which is greater than 0.6. Thus, B_5 is a faulty component.
4. Similarly, the measured value of T_1 is 0.2363, and T_1 is a non-faulty component.

4.2.3. Case 3

A fault occurs at T_1. Tp_1m operates, and then CB_{44} and CB_{51} trip. However, the timestamp of the CB_{51} alarm message is incorrect due to transmission delays. The alarm messages are briefly described as $Tp_1m(0)$, $CB_{44}(25)$, and $CB_{51}(70)$. The fault diagnosis process is as follows:

1. *CBS* = {CB_{44}, CB_{51}} can be obtained from the alarm message. Traverse *CBS* and search for suspected faulty components. There is a subset COM_{44} = {B_4, T_1, B_5, L_{CL}}, a subset COM_{51} = {B_5, T_1, L_{CXI}, B_4, L_{CXII}, L_{CM}, L_{SCI}, L_{SCII}}, and a total set *COMS* = {T_1, B_4, B_5}.
2. T_1 is selected for fault diagnosis. The $\boldsymbol{\alpha}^0_{p(11)}$, $\boldsymbol{T}^0_{p(11)}$, $\boldsymbol{\alpha}^0_{p(12)}$, and $\boldsymbol{T}^0_{p(12)}$ of the fault diagnosis model for the CB_{44} and CB_{51} subnets are as follows.

$$\begin{cases} \boldsymbol{\alpha}^0_{p(11)} = [0.9833, 0.2, 0.2, 0.7756, 0.2, 0.2, 0, 0, 0, 0]^{\mathrm{T}} \\ \boldsymbol{T}^0_{p(11)} = [[25, 25], [25, 25], \varnothing, [0, 0], \varnothing, \varnothing, \varnothing, \varnothing, \varnothing, \varnothing]^{\mathrm{T}} \end{cases} \tag{40}$$

$$\begin{cases} \boldsymbol{\alpha}^0_{p(12)} = [0.9833, 0.2, 0.2, 0.7756, 0.2, 0.2, 0, 0, 0, 0]^{\mathrm{T}} \\ \boldsymbol{T}^0_{p(12)} = [[70, 70], [70, 70], \varnothing, [0, 0], \varnothing, \varnothing, \varnothing, \varnothing, \varnothing, \varnothing]^{\mathrm{T}} \end{cases} \tag{41}$$

3. The diagnosis results for the CB_{44} subnet are $\alpha_{p10(11)} = 0.8797$ and $T_{p10(11)} = [-40, -10]$. The diagnosis results of the CB_{51} subnet are $\alpha_{p10(12)} = 0.8795$ and $T_{p10(12)} = [-40, 40]$. The diagnosis results of T_{1213} are $\alpha_{(1)} = 0.8795$ and $T_{(1)} = [-40, -10]$, and its measured value $\eta_{(1)} = 0.9156$, which is greater than 0.6. Thus, T_1 is a faulty component.
4. Similarly, the measured values of B_4 and B_5 are 0.1857 and 0.1881, respectively, and they are non-faulty components.

4.3. Comparison Analysis with Other Methods

4.3.1. Case Result Comparisons

The proposed method and other existing methods are used for fault diagnosis in Cases 1–16, and the diagnosis results are shown in Table 3. The methods in [13,17,18,23] do not consider the temporal features of alarm messages, whereas the methods in [20–22] consider temporal features.

Table 3. Fault diagnosis results of the proposed method and existing methods for cases 1–16.

No.	Suspected Faulty Components		Fault Diagnosis Results								Faulty Components
	[16,21,22]	This Study	[13]	[23]	[17]	[18]	[20]	[21]	[22]	This Study	
1	B_{18}	B_{18}	B_{18}	B_{18}	B_{18}	B_{18}	B_{18}	B_{18}	B_{18}	B_{18}	B_{18}
2	L_{0318}, L_{1718}, B_{18}	L_{0318}, L_{1718}, B_{18}	L_{0318}, B_{18}	L_{0318}	L_{0318}, B_{18}	L_{0318}, B_{18}	L_{0318}	L_{0318}, B_{18}	L_{0318}	L_{0318}	L_{0318}
3	-	T_{1213}, B_{12}, B_{13}, L_{1314}, L_{1013}	T_{1213}	-	T_{1213}	-	-	T_{1213}	-	T_{1213}	T_{1213}
4	-	B_{18}, B_{17}, L_{1718}, L_{1727}, L_{1617}	B_{18}	-	B_{18}	B_{18}	B_{18}	B_{18}	B_{18}	B_{18}	B_{18}
5	L_{0318}, B_{03}	B_{18}, L_{1718}	B_{18}	B_{18}	B_{18}	B_{18}	B_{18}	B_{18}	B_{18}	B_{18}	B_{18}
6	B_{03}	B_{03}	B_{03}	-	-	-	-	-	B_{03}	B_{03}	B_{03}
7	B_{03}, L_{0203}, L_{0304}, L_{0318}	B_{03}, L_{0203}, L_{0304}, L_{0318}	B_{03}, L_{0203}, L_{0304}, L_{0318}	B_{03}	B_{03}, L_{0203}, L_{0304}, L_{0318}	B_{03}, L_{0203}, L_{0304}, L_{0318}	B_{03}	B_{03}	B_{03}	B_{03}	B_{03}
8	L_{0318}	L_{0318}	L_{0318}	L_{0318}	L_{0318}	L_{0318}	L_{0318}	-	L_{0318}	L_{0318}	L_{0318}
9	L_{0318}, L_{1718}, B_{18}	L_{0318}, L_{1718}, B_{18}	L_{0318}, B_{18}	-	L_{0318}, B_{18}	L_{0318}, B_{18}	-	B_{18}	L_{0318}	L_{0318}	L_{0318}
10	-	L_{0318}, L_{1718}, B_{18}, B_{17}	L_{0318}, B_{18}, L_{1718}	-	L_{0318}, B_{18}	L_{0318}, B_{18}	-	B_{18}	L_{0318}	L_{0318}	L_{0318}
11	-	T_{1213}, B_{12}, B_{13}, L_{1314}, L_{1013}	T_{1213}	-	T_{1213}	-	-	T_{1213}	-	T_{1213}	T_{1213}
12	T_{1213}, B_{13}, L_{1314}, L_{1013}	T_{1213}, B_{13}, L_{1314}, L_{1013}	T_{1213}, B_{13}, L_{1314}, L_{1013}	-	T_{1213}, B_{13}, L_{1314}, L_{1013}	B_{13}, L_{1314}, L_{1013}	-	T_{1213}	-	T_{1213}	T_{1213}
13	B_{18}, L_{1718}	L_{0318}, L_{1718}, B_{17}, B_{18}	L_{1718}	L_{1718}	L_{1718}	L_{1718}	L_{1718}	L_{1718}	L_{1718}	L_{0318}, L_{1718}	L_{0318}, L_{1718}
14	L_{0318}, L_{1718}, B_{17}, B_{18}	L_{0318}, L_{1718}, B_{17}, B_{18}	L_{0318}, B_{17}, B_{18}	L_{0318}, B_{17}	L_{0318}, B_{17}	L_{0318}, B_{17}	L_{0318}, B_{17}	L_{0318}, B_{17}	L_{0318}, B_{17}	L_{0318}, B_{17}	L_{0318}, B_{17}
15	B_{14}	B_{03}, B_{14}	B_{14}	B_{14}	B_{14}	B_{14}	B_{14}	B_{14}	B_{14}	B_{03}, B_{14}	B_{03}, B_{14}
16	B_{18}, L_{0318}, L_{1718}, T_{1213}	B_{18}, L_{0318}, L_{1718}, T_{1213}, B_{12}, B_{13}	B_{18}, L_{0318}, L_{1718}, T_{1213}	B_{18}	B_{18}, L_{0318}, L_{1718}	B_{18}, L_{0318}, L_{1718}	B_{18}	B_{18}	B_{18}	B_{18}, T_{1213}	B_{18}, T_{1213}

Existing methods must identify the outage area to reduce suspected faulty components and improve the efficiency of the fault diagnosis. Outage and active areas are separated using tripped CBs. Once the alarm message of boundary CB is lost (Cases 3 and 4), the

outage area cannot be determined. Existing methods must diagnose all the components in the power system. In complex faults (Cases 13 and 15), the existing methods only search for the outage area with complete CB alarm messages. They failed to identify the faulty components (L_{0318} in Case 13 and B_{03} in Case 15) in the outage area without an alarm message regarding the boundary CBs. Therefore, this study proposes a search method for suspected faulty components by considering the missing alarm messages of boundary CBs. Suspected faulty components corresponding to tripped CBs are searched for to form subsets. These subsets complement and verify each other to avoid missing faulty components in case of missing CB alarms. Moreover, this method does not need to traverse the entire power system topology, reduce the scope of the topology search, or improve the fault diagnosis efficiency.

In [13], the confidence degrees are corrected according to the quantitative relationship between PRs and CBs. The method in [13] can avoid the misdiagnosis problem when the key alarm message is missing (Cases 6 and 16). However, the adjacent components are misdiagnosed when the remote backup PR and its CBs operate. For example, Lp_{1718}s and CB_{1718} were operational in Case 2. Because they are also the remote backup PR and corresponding CB of B_{18}, the B_{18} diagnosis result exceeded the threshold in [13], and B_{18} was misdiagnosed as a faulty component.

The method in [23] has a high diagnosis accuracy when the alarm message is complete. However, this method considers the minimum confidence degree in PRs and CBs as the diagnosis result for suspected faulty components. Therefore, when an alarm message is missing (Cases 10–12), this method cannot diagnose the fault component with the missing alarm message, and the fault tolerance is poor.

The methods in [17,18] can diagnose faulty components in most cases. However, misdiagnosis and missed diagnosis occur during remote backup PR operation (Cases 10 and 16) and missing alarm messages (Cases 6 and 16), respectively. The cause of the misdiagnosis is the same as that in [13], without considering the remote backup PR and CB of adjacent components. The main reason for the missed diagnosis is that the bus PR and transformer PR are associated with multiple CBs simultaneously, and the missing alarm message of the bus PR and transformer PR will seriously affect the fault diagnosis results of the faulty bus and transformer.

The accuracy of fault diagnosis is improved using temporal features and reasoning in [20,21]. However, only the PR and CB confidence degrees that do not satisfy the temporal constraints are punished, and there are no corresponding compensation measures. When the alarm message is missing, or the timestamp is incorrect, there is a problem of missed diagnosis, and the fault tolerance must be improved [20,21].

In reference [20], alarm messages are categorized as valid or invalid based on their relationship and temporal constraints with PRs and CBs, with valid alarms being assigned confidence degrees. However, the method in [20] classifies the alarm message of CB_{0318} as invalid (with a confidence degree of 0.2) in Case 9, because CB_{0318} has no corresponding PR alarm message. The confidence degree of L_{0318} is 0.3836 (lower than the threshold in [20]), and L_{0318} is diagnosed as a non-faulty component. The method in [21] corrects the confidence degrees of PRs and CBs that do not meet the temporal constraint in the sequence of "Fault time—PR operation time—CB trip time". If the timestamp of a PR alarm message is incorrect, this method determines that the PR and the corresponding CB do not meet their temporal constraints, resulting in a missed diagnosis. For example, in Case 8, because the timestamp of Lp_{1803}p is incorrect, Lp_{1803}p and CB_{1803} do not meet the temporal constraints, their confidence degrees are corrected to 0, and L_{0318} is diagnosed as a non-faulty component. In addition, the temporal reasoning in [21] defaults the fault time to zero, but the alarm message does not include the fault time; thus, determining the fault time is a problem that this method must solve.

Combining the above case comparisons, the accuracy and fault tolerance comparison of the proposed method with other methods is shown in Table 4. The proposed method deduces the fault time by the operation times of PRs and CBs, adjusting the confidence

degrees of the suspected faulty components by using a measure function and fault time. Furthermore, this study addresses the misdiagnosis problem in the case of neighboring components configured with the same backup protection and incorrect operations of the PRs and CBs. It also maintains diagnostic precision even when alarm messages of the boundary CB or main PRs of the bus and transformer are absent. Temporal errors do not affect the temporal reasoning of PRs and CBs. In contrast, the temporal results of different CB subnets are cross-verified, enhancing the reliability of temporal reasoning and adjustments made by the measure function. The comparison of fault results demonstrates that this study makes full use of temporal features and reasoning in complex fault scenarios, effectively enhancing the accuracy and fault tolerance of fault diagnosis.

Table 4. Comparison of the proposed method with the existing methods.

	[13]	[23]	[17]	[18]	[20]	[21]	[22]	**This Study**
Consideration of temporal features	No	No	No	No	Yes	Yes	Yes	Yes
Consideration of neighboring components configured with the backup protection	No	Yes	No	No	Yes	Yes	Yes	Yes
Consideration of incorrect operations of the PRs and CBs	Yes	Yes	Yes	Yes	Yes	Yes	Yes	Yes
Consideration of missing alarms of the boundary CBs	No	No	No	No	No	No	No	Yes
Consideration of the uncertainty of alarm messages	Yes	No	Not considering the main protection of the bus and transformer	Not considering the main protection of the bus and transformer	Not considering the main protection of the bus and transformer	Not considering the main protection of the bus and transformer	Yes	Yes
Consideration of timing errors	No	No	Yes	No	Yes	No	Yes	No
Accuracy and fault tolerance	General	Poor	General	General	Good	Good	Excellent	Excellent

4.3.2. Performance Comparison

Table 5 compares the performance of the proposed method with the existing methods in [10,20–22,24] that consider temporal features.

In [24], temporal constraints are added to the loss function of the analytical model to solve the multi-solution problem. However, more variables increase the number of calculations and reduce the convergence speed of the optimization algorithm. The action event coding and the temporal rule bases of PRs and CBs are required in [10,20,21]. After a fault occurs, the alarm message is matched with the rule base to determine an effective alarm message and modify its confidence degree. The temporal matching and reasoning processes of the fault diagnosis model are independent of each other [10,20,21]. The fault diagnosis process is complex, and the number of calculations is large, which restricts online applications. The rTSSNPS system also implements correlation reasoning between confidence degrees and temporal constraints; however, its reasoning method is more complex and does not realize fault diagnosis of transformer components [22].

Table 5. Performance comparison between the proposed method and existing methods.

Method	Fault Diagnosis Models	Search Method for Suspected Faulty Components	Calculation Tasks	Calculation Methods and Calculation Amounts	Performance
This study	No need to build separate models No need to adjust diagnosis models for topology changes	Search for suspected faulty components configured the tripped CBs	Correlation reasoning between confidence degrees and temporal constraints	Matrix operation with a calculation amount of $\mu\nu$	Simple reasoning and calculation principles Strong generality and adaptability of the fault diagnosis model
[24]	Construction of the objective function based on the alarm message	Search the outage area to identify suspected faulty components	Fault hypothesis with the minimum loss value	Look-up table and optimization algorithm with a calculation amount of $2^{\mu}v$	Relatively slow convergence speed High calculation complexity
[10]	Individual construction of fault diagnosis models for suspected faulty components. Need for reconstruction of models based on topology changes for fault diagnosis.		Temporal matching of alarm messages Fuzzy reasoning of confidence degrees	Event correlation, look-up table, and matrix operation with a calculation amount of $\mu^2\nu$	Independence of confidence reasoning and temporal reasoning processes High complexity in the alarm message association and temporal matching process
[20]			Temporal matching and classification of alarm messages Fuzzy reasoning of confidence degrees	Event correlation, look-up table, and matrix operation with a calculation amount of $2\mu\nu$	
[21]			Temporal matching of alarm messages Fuzzy reasoning of confidence degrees	Event correlation, look-up table, and matrix operation with a calculation amount of $2\mu\nu$	
[22]			Correlation reasoning between confidence degrees and temporal constraints	Matrix operation with a calculation amount of $\mu\nu$	Relatively complex reasoning and calculation process in fault diagnosis High efficiency in diagnosis Lack of consideration for transformer fault diagnosis

Note: μ denotes the number of received alarm messages, and ν denotes the number of suspected faulty components.

Compared to the above methods, the ITFRSNP system and its reasoning method do not require the construction of corresponding event codes and temporal rule libraries for each suspected fault component. The proposed method avoids complex temporal matching and confidence correction processes in temporal reasoning. Simultaneously, the fault diagnosis principle based on the general fault diagnosis model simplifies the association reasoning steps of the confidence degrees and temporal constraints, thus reducing the complexity of the reasoning algorithm and improving fault diagnosis efficiency.

In addition, the above methods do not fully consider the impact of the missing boundary CB alarm message on fault diagnosis results and efficiency. Once the boundary CB alarm message is lost, it is not possible to form an outage area when diagnosing a single fault. It is necessary to diagnose all the components in the power grid with a significant

amount of computation and reduced fault efficiency. Moreover, when diagnosing multiple faults, only the outage area with complete boundary CB alarm messages can be correctly identified, and faulty components located in the unrecognized outage area are missed, thereby reducing the fault diagnosis accuracy.

The proposed method suspected faulty components within the isolation range of tripped CBs based on the operation logic of the PRs and CBs. Compared with other methods, the search algorithm for suspected fault components in this study does not need to traverse the whole grid topology, thus enhancing search efficiency. Meanwhile, it can narrow down the diagnosis scope of a single fault without missing faulty components in multiple faults in the case of missing alarm messages of boundary CBs. In the case of rejections and missing/false alarm messages, this study combines confidence degrees and temporal constraints for fault diagnosis to reduce misdiagnoses and missed diagnoses.

Owing to the different types and topologies of the components, it is necessary for [10,20–22,24] to build the corresponding fault diagnosis model for each component separately. The structure and parameters of the fault diagnosis model are reconstructed or adjusted according to topology changes. In contrast to the above methods, this study can directly use a general fault diagnosis model to diagnose the subnets of suspected faulty components and fuse the diagnosis results of each subnet to diagnose the faulty components. For example, as shown in Figure 7, L_{0304} is out of operation because of maintenance, the number of adjacent lines of B_{03} and B_{04} is reduced, and the number of remote backup PRs of L_{0203} and L_{0318} is reduced. If a fault occurs in B_{03}, the proposed method diagnoses the CB_{0302} and CB_{0318} subnets of B_{03}. If L_{0203} (L_{0318}) fails, the fault diagnosis process in this study automatically searches for remote backup PRs and CBs of L_{0203} (L_{0318}) and their alarm messages. The input of the general fault diagnosis model of the corresponding subnet is then adjusted according to (21).

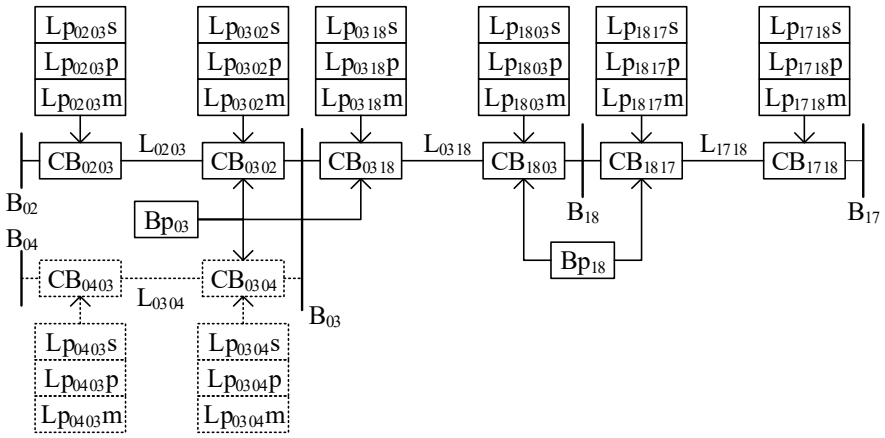


Figure 7. Schematic diagram of power system topology change.

Taking B_{03} and L_{0318} in Figure 7 as examples, the fault diagnosis models are constructed using the methods in [20–22] and compared with the proposed method. The numbers of proposition neurons α_p and rule neurons α_r in the fault diagnosis models are listed in Table 6. Hierarchical modeling is employed in [20–22], which can flexibly adjust the hierarchical structure of the fault model according to topology changes; however, more neurons are needed to link the sub-models of different hierarchies for fault diagnosis. As more neurons require more synapses for association, the size of the fault diagnosis model increases, and the structure becomes more complex. After the L_{0304} outage, the remote backup protection of adjacent components is reduced, and the fault diagnosis models of the above methods must delete the corresponding neurons. If L_{0304} restarts operation, it is necessary to add the corresponding neurons in the fault diagnosis models. The structure, input matrix, and output matrix of the fault diagnosis model are changed. This illustrates that topology changes have an impact on the fault diagnosis models of the existing methods;

in particular, the changes are most pronounced for the fault diagnosis models of the bus. Therefore, existing methods need to adjust the parameters of the fault diagnosis model according to topology changes to ensure the accuracy of the fault diagnosis.

Table 6. The number of neurons in the fault diagnosis models.

Components		This Study		[20]		[21]		[22]	
		α_p	α_r	α_p	α_r	α_p	α_r	α_p	α_r
Before L_{0304} outage	B_{03}	10	7	21	9	25	10	25	16
	L_{0318}	10	7	20	8	35	11	23	16
After L_{0304} outage	B_{03}	10	7	14	6	16	7	17	11
	L_{0318}	10	7	18	8	29	9	21	15

This study defines a CB subnet and proposes a general fault diagnosis model. The PRs and CBs of faulty components are decomposed into multiple CB subnets with the same relay protection configurations, and the general fault diagnosis model is invoked through the diagnosis process to diagnose the CB subnets. This study does not need to build a diagnosis model for a single component online, and the general fault diagnosis model has a simple structure that can be applied to the fault diagnosis of various components. Moreover, the general fault diagnosis model and its reasoning process can automatically adapt to topological changes and simplify the fault diagnosis modeling process.

5. Conclusions

This study proposes a fault diagnosis method based on the ITFRSNP system and a fault diagnosis principle based on a general fault diagnosis model. First, this study proposes the ITFRSNP system, which contains new rule neurons and reasoning methods to realize correlation reasoning of confidence degrees and temporal constraints. This provides a theoretical basis for a general fault diagnosis model. Then, the concept of the CB subnet is defined according to the configuration of the CBs and corresponding PRs. A general fault diagnosis model based on the ITFRSNP system is constructed for the CB subnet. The subnets of the suspected faulty components are diagnosed using the general fault diagnosis model. The diagnosis results of the subnets are fused to determine faulty components. This study also proposes a new search method for suspected faulty components, which avoids the expanded diagnosis scope and incorrect diagnosis. Finally, the effectiveness and reliability of this method are verified and analyzed using a case simulation.

The proposed method can diagnose fault components and time in complex fault scenarios with high accuracy and tolerance. Additionally, the general fault diagnosis model effectively accommodates a variety of components and topological alterations, demonstrating broad applicability and flexibility while streamlining the modeling process. The search algorithm for suspected faulty components reduces the scope of the topology search without missing the faulty components. Owing to its reliability, simplicity, and computational efficiency, the method fulfills the demands of online fault diagnosis, showcasing promising application potential.

The proposed method encounters challenges in diagnosing faults in complex wiring connections, such as double bus and 3/2 wiring connections. In double bus connections, CBs are interconnected between buses, whereas in 3/2 wiring connections, CBs are linked directly. The relay protection configurations in these complex wiring connections are different from those in the CB subnet in this study. Therefore, the proposed method is not applicable to the fault diagnosis of double bus and 3/2 wiring connections. Future research will concentrate on analyzing relay protection configuration and operation logic within complex wiring connections, developing a topology search method, a general fault diagnosis model and a fault diagnosis process to realize the fault diagnosis of complex wiring.

Author Contributions: Conceptualization, N.S. and Q.C.; data curation, N.S. and C.Y.; formal analysis, N.S., D.X. and Y.S.; funding acquisition, Q.C.; methodology, N.S., C.Y. and D.X.; project administration, Q.C.; software, N.S.; validation, N.S. and Q.C.; visualization, N.S. and Y.S.; writing original draft, N.S.; writing review and editing, N.S., C.Y., D.X. and Y.S. All authors have read and agreed to the published version of the manuscript.

Funding: This work was supported by the National Natural Science Foundation of China, under Grant 51877123.

Institutional Review Board Statement: Not applicable.

Informed Consent Statement: Not applicable.

Data Availability Statement: The data presented in this study are available in the article.

Conflicts of Interest: The authors declare no conflicts of interest. The funders had no role in the design of the study; in the collection, analyses, or interpretation of data; in the writing of the manuscript or in the decision to publish the results.

References

1. Kaluder, S.; Fekete, K.; Jozsa, L.; Klaic, Z. Fault Diagnosis and Identification in the Distribution Network Using the Fuzzy Expert System. *Eksploat. I Niezawodn.-Maint. Reliab.* **2018**, *20*, 621–629. [CrossRef]
2. Perez, R.; Inga, E.; Aguila, A.; Vasquez, C.; Lima, L.; Viloria, A.; Henry, M.-A. Fault Diagnosis on Electrical Distribution Systems Based on Fuzzy Logic. In Proceedings of the 9th International Conference on Swarm Intelligence (ICSI), Shanghai, China, 17–22 July 2018; pp. 174–185.
3. Xiong, G.; Shi, D.; Zhang, J.; Zhang, Y. A binary coded brain storm optimization for fault section diagnosis of power systems. *Electr. Power Syst. Res.* **2018**, *163*, 441–451. [CrossRef]
4. Wang, S.; Zhao, D.; Yuan, J.; Li, H.; Gao, Y. Application of NSGA-II Algorithm for fault diagnosis in power system. *Electr. Power Syst. Res.* **2019**, *175*, 105893. [CrossRef]
5. Wang, S.-P.; Zhao, D.-M. A Hierarchical Power Grid Fault Diagnosis Method Using Multi-Source Information. *IEEE Trans. Smart Grid* **2020**, *11*, 2067–2079. [CrossRef]
6. Yang, Q.; Le Blond, S.; Aggarwal, R.; Wang, Y.; Li, J. New ANN method for multi-terminal HVDC protection relaying. *Electr. Power Syst. Res.* **2017**, *148*, 192–201. [CrossRef]
7. Han, J.; Miao, S.; Li, Y.; Yang, W.; Yin, H. Faulted-Phase classification for transmission lines using gradient similarity visualization and cross-domain adaption-based convolutional neural network. *Electr. Power Syst. Res.* **2021**, *191*, 106876. [CrossRef]
8. Han, Y.; Tong, X. Power System Fault Diagnosis Based on Dynamic Reasoning Chain. *Power Syst. Technol.* **2017**, *41*, 1315–1323.
9. Lin, S.; Chen, X.; Wang, Q. Fault diagnosis model based on Bayesian network considering information uncertainty and its application in traction power supply system. *IEEJ Trans. Electr. Electron. Eng.* **2018**, *13*, 671–680. [CrossRef]
10. Zhang, Y.; Zhang, Y.; Wen, F.; Chung, C.Y.; Tseng, C.-L.; Zhang, X.; Zeng, F.; Yuan, Y. A fuzzy Petri net based approach for fault diagnosis in power systems considering temporal constraints. *Int. J. Electr. Power Energy Syst.* **2016**, *78*, 215–224. [CrossRef]
11. Kiaei, I.; Lotfifard, S. Fault Section Identification in Smart Distribution Systems Using Multi-Source Data Based on Fuzzy Petri Nets. *IEEE Trans. Smart Grid* **2020**, *11*, 74–83. [CrossRef]
12. Yuan, C.; Liao, Y.; Kong, L.; Xiao, H. Fault diagnosis method of distribution network based on time sequence hierarchical fuzzy petri nets. *Electr. Power Syst. Res.* **2021**, *191*, 106870. [CrossRef]
13. Zhang, X.; Yue, S.; Zha, X. Method of power grid fault diagnosis using intuitionistic fuzzy Petri nets. *IET Gener. Transm. Distrib.* **2018**, *12*, 295–302. [CrossRef]
14. Wang, J.; Peng, H.; Tu, M.; Perez-Jimenez, J.M.; Shi, P. A Fault Diagnosis Method of Power Systems Based on an Improved Adaptive Fuzzy Spiking Neural P Systems and PSO Algorithms. *Chin. J. Electron.* **2016**, *25*, 320–327. [CrossRef]
15. Rong, H.; Yi, K.; Zhang, G.; Dong, J.; Paul, P.; Huang, Z. Automatic Implementation of Fuzzy Reasoning Spiking Neural P Systems for Diagnosing Faults in Complex Power Systems. *Complexity* **2019**, *2019*, 2635714. [CrossRef]
16. Wang, T.; Zhang, G.; Zhao, J.; He, Z.; Wang, J.; Perez-Jimenez, M.J. Fault Diagnosis of Electric Power Systems Based on Fuzzy Reasoning Spiking Neural P Systems. *IEEE Trans. Power Syst.* **2015**, *30*, 1182–1194. [CrossRef]
17. Peng, H.; Wang, J.; Ming, J.; Shi, P.; Perez-Jimenez, M.J.; Yu, W.; Tao, C. Fault Diagnosis of Power Systems Using Intuitionistic Fuzzy Spiking Neural P Systems. *IEEE Trans. Smart Grid* **2018**, *9*, 4777–4784. [CrossRef]
18. Wang, J.; Peng, H.; Yu, W.; Ming, J.; Perez-Jimenez, M.J.; Tao, C.; Huang, X. Interval-valued fuzzy spiking neural P systems for fault diagnosis of power transmission networks. *Eng. Appl. Artif. Intell.* **2019**, *82*, 102–109. [CrossRef]
19. Liu, W.; Wang, T.; Zang, T.; Huang, Z.; Wang, J.; Huang, T.; Wei, X.; Li, C. A Fault Diagnosis Method for Power Transmission Networks Based on Spiking Neural P Systems with Self-Updating Rules considering Biological Apoptosis Mechanism. *Complexity* **2020**, *2020*, 2462647. [CrossRef]
20. Huang, K.; Wang, T.; He, Y.; Zhang, G.; Pérez-Jiménez, M.J. Temporal fuzzy reasoning spiking neural P systems with real numbers for power system fault diagnosis. *J. Comput. Theor. Nanosci.* **2016**, *13*, 3804–3814. [CrossRef]

21. Wang, T.; Wei, X.; Wang, J.; Huang, T.; Peng, H.; Song, X.; Valencia Cabrera, L.; Perez-Jimenez, M.J. A weighted corrective fuzzy reasoning spiking neural P system for fault diagnosis in power systems with variable topologies. *Eng. Appl. Artif. Intell.* **2020**, *92*, 103680. [CrossRef]
22. Lin, D. A fault diagnosis method for power grid based on time sequential spiking neural P systems. *New Tech. New Products China.* **2022**, *2*, 1–7.
23. Xiong, G.; Shi, D.; Zhu, L.; Duan, X. A New Approach to Fault Diagnosis of Power Systems Using Fuzzy Reasoning Spiking Neural P Systems. *Math. Probl. Eng.* **2013**, *2013*, 815352. [CrossRef]
24. Guo, W.; Wen, F.; Ledwich, G.; Liao, Z.; He, X.; Huang, J. A new analytic approach for power system fault diagnosis employing the temporal information of alarm messages. *Int. J. Electr. Power Energy Syst.* **2012**, *43*, 1204–1212. [CrossRef]

Disclaimer/Publisher's Note: The statements, opinions and data contained in all publications are solely those of the individual author(s) and contributor(s) and not of MDPI and/or the editor(s). MDPI and/or the editor(s) disclaim responsibility for any injury to people or property resulting from any ideas, methods, instructions or products referred to in the content.